⌘ *Author's Choice*

THE JOURNAL OF BIOLOGICAL CHEMISTRY VOL. 290, NO. 47, pp. 28214–28230, November 20, 2015

Routes of Ca^{2+} Shuttling during Ca^{2+} Oscillations

FOCUS ON THE ROLE OF MITOCHONDRIAL Ca^{2+} HANDLING AND CYTOSOLIC Ca^{2+} BUFFERS[*S]

Received for publication, May 5, 2015, and in revised form, September 9, 2015 Published, JBC Papers in Press, September 22, 2015, DOI 10.1074/jbc.M115.663179

László Pecze[1], **Walter Blum, and Beat Schwaller**

From Anatomy, Department of Medicine, University of Fribourg, Route Albert-Gockel 1, CH-1700 Fribourg, Switzerland

Background: Ca^{2+} oscillations in mesothelial cells depend on Ca^{2+} influx.
Results: However, the "lanthanum insulation method" renders the oscillations independent of extracellular Ca^{2+}.
Conclusion: Multiple pathways of Ca^{2+} shuttling are operating simultaneously during Ca^{2+} oscillations.
Significance: Experimental and mathematical approaches shed light on the mechanism of Ca^{2+} oscillations.

In some cell types, Ca^{2+} oscillations are strictly dependent on Ca^{2+} influx across the plasma membrane, whereas in others, oscillations also persist in the absence of Ca^{2+} influx. We observed that, in primary mesothelial cells, the plasmalemmal Ca^{2+} influx played a pivotal role. However, when the Ca^{2+} transport across the plasma membrane by the "lanthanum insulation method" was blocked prior to the induction of the serum-induced Ca^{2+} oscillations, mitochondrial Ca^{2+} transport was found to be able to substitute for the plasmalemmal Ca^{2+} exchange function, thus rendering the oscillations independent of extracellular Ca^{2+}. However, in a physiological situation, the Ca^{2+}-buffering capacity of mitochondria was found not to be essential for Ca^{2+} oscillations. Moreover, brief spontaneous Ca^{2+} changes were observed in the mitochondrial Ca^{2+} concentration without apparent changes in the cytosolic Ca^{2+} concentration, indicating the presence of a mitochondrial autonomous Ca^{2+} signaling mechanism. In the presence of calretinin, a Ca^{2+}-buffering protein, the amplitude of cytosolic spikes during oscillations was decreased, and the amount of Ca^{2+} ions taken up by mitochondria was reduced. Thus, the increased calretinin expression observed in mesothelioma cells and in certain colon cancer might be correlated to the increased resistance of these tumor cells to proapoptotic/pronecrotic signals. We identified and characterized (experimentally and by modeling) three Ca^{2+} shuttling pathways in primary mesothelial cells during Ca^{2+} oscillations: Ca^{2+} shuttled between (i) the endoplasmic reticulum (ER) and mitochondria, (ii) the ER and the extracellular space, and (iii) the ER and cytoplasmic Ca^{2+} buffers.

The calcium ion (Ca^{2+}) is a universal intracellular messenger that controls a diverse range of cellular processes including cell proliferation, apoptosis, fertilization, neurotransmitter release, and heartbeat among many others (1). Ca^{2+} pumps in the plasma membrane (plasma membrane Ca^{2+}-ATPase) and in endoplasmic reticulum (ER)[2] membranes (SERCA) are responsible for the low cytosolic (c_{cyt}) and nuclear free Ca^{2+} concentrations (c_{nucl}) (50–100 nM) compared with the free Ca^{2+} concentrations in the extracellular space (1–2 mM) and the ER lumen (c_{ER}) (100–500 μM). At rest, the free Ca^{2+} concentration in the mitochondrial matrix (c_{mito}) is close to the resting c_{cyt}, but it rises to 20–30 μM during stimulation, *e.g.* in motor nerve terminals in *Drosophila melanogaster* (2). Cell activation in a wide range of cell types results in Ca^{2+} oscillations and in transient waves of increased c_{cyt} (3–6). These oscillations (or waves) are not restricted to c_{cyt}, but also c_{nucl} (7), c_{ER} (8), and c_{mito} show Ca^{2+} oscillations (9). The spatial extent of the oscillatory Ca^{2+} signal is also important. (i) In astrocytes, the area of Ca^{2+} oscillations is sometimes restricted to only one protrusion regulating the release of gliotransmitters; *i.e.* different oscillatory frequencies can coexist at the same time within the same cell (10). (ii) In *Xenopus laevis* oocytes, regenerative spiral waves of release of free Ca^{2+} spread through the entire cell (11). (iii) Intercellular Ca^{2+} waves spreading via gap junctions occur in rat liver epithelial cells upon mechanical stimulation (12).

In cells maintained *in vitro*, serum starvation followed by readministration leads to intracellular Ca^{2+} signals, most often in the form of oscillations (13, 14). The precise mechanism(s) leading to these oscillations is poorly understood because serum contains a large number of known and as yet unidentified growth factors and mitogenic compounds, all potentially participating in this oscillatory activity (15). In Swiss 3T3 cells, serum-induced Ca^{2+} changes are essential but not sufficient to induce NF-κB activation and subsequent DNA synthesis (16). In some cell types, Ca^{2+} oscillations even persist in the absence of Ca^{2+} influx across the plasma membrane (3, 4), whereas in others, Ca^{2+} oscillations strictly depend on Ca^{2+} influx (5, 8).

* This work was partially supported by Swiss National Science Foundation Grants 130680 and 147697 (Sinergia) (to B. S.). The authors declare that they have no conflicts of interest with the contents of this article.

[S] This article contains a supplemental Excel document showing an example of mathematical simulation.
[1] To whom correspondence should be addressed. Tel.: 41-26-300-85-11; Fax: 41-26-300-97-33; E-mail: laszlo.pecze@unifr.ch.

[2] The abbreviations used are: ER, endoplasmic reticulum; SERCA, sarco/endoplasmic reticulum Ca^{2+}-ATPase; c_{cyt}, cytosolic free Ca^{2+} concentration; c_{nucl}, nuclear free Ca^{2+} concentration; c_{ER}, free Ca^{2+} concentration in the ER lumen; c_{mito}, free Ca^{2+} concentration in the mitochondrial matrix; MCU, mitochondrial calcium uniporter; CCCP, carbonyl cyanide *m*-chlorophenylhydrazone; prMC, primary mouse mesothelial cells; EBFP, enhanced blue fluorescent protein; $InsP_3R$, inositol trisphosphate receptor; $InsP_3$, inositol trisphosphate; $\Delta\Psi$, mitochondrial membrane potential; BAPTA, 1,2-bis(2-aminophenoxy)ethane-*N*,*N*,*N*′,*N*′-tetraacetic acid; AM, acetoxymethyl ester; CR, calretinin; qRT-PCR, quantitative RT-PCR; ROI, region of interest.

Mitochondria influence cytosolic Ca^{2+} oscillations in at least two ways. First, mitochondria produce ATP, which is required for SERCA and plasma membrane Ca^{2+}-ATPase function, that results in Ca^{2+} extrusion and thus lowering of c_{cyt}. Second, during c_{cyt} oscillations, c_{mito} also manifests oscillations, indicative of a role of mitochondria in shaping and/or modulating c_{cyt} oscillations (9). Ca^{2+} uptake into the mitochondria is determined by both the large negative voltage (−150 to −180 mV) across the inner membrane that results from the proton pumping by the respiratory chain and the Ca^{2+} concentration gradient between the cytoplasm and matrix (17). The mitochondrial calcium uniporter (MCU) is the key player responsible for the uptake of Ca^{2+} by mitochondria (18). The MCU has a rather low Ca^{2+} affinity and operates over a micromolar range of cytosolic Ca^{2+}.

To address these questions, we performed lanthanum (La^{3+}) insulation experiments where both the Ca^{2+} influx and efflux across the plasma membrane are blocked (19). We hypothesized that under these experimental conditions mitochondria serving as a Ca^{2+} store/source might substitute for this function normally exerted by the extracellular space. Using a genetically encoded Ca^{2+} indicator targeted to the mitochondria, we managed to verify this assumption *in vitro*. In addition, we investigated the effects of the following compounds on c_{cyt} oscillations and mitochondrial Ca^{2+} handling: the proton uncoupler carbonyl cyanide *m*-chlorophenylhydrazone (CCCP), the mitochondrial Na^+/Ca^{2+} blocker CGP-37157, the mitochondrial MCU blocker Ru-360, and finally the "Ca^{2+}-buffering" protein calretinin. Based on the experimental findings, we built a mathematical model for Ca^{2+} oscillations taking into account the various processes implicated in these oscillations.

Materials and Methods

Reagents—Thapsigargin, $LaCl_3$, and EGTA were purchased from Sigma-Aldrich. CGP-37157 and BAPTA-AM were obtained from Tocris Bioscience (Bristol, UK). Ru-360 was purchased from Calbiochem, and Rhodamine 123 was from Invitrogen. EGTA-AM and tetramethylrhodamine methyl ester were purchased from AAT Bioquest (Sunnyvale, CA). CGP-37157 was dissolved in pure ethanol as 100 mM stock solutions. Thapsigargin and Rhodamine 123 were dissolved as 100 mM stock solutions in DMSO. BAPTA-AM and EGTA-AM were dissolved as 30 mM stock solutions in DMSO. $LaCl_3$ was dissolved in double distilled water. The final concentrations of the solvents were <0.1% in all experimental solutions. At these concentrations, the solvents did not modify the evoked Ca^{2+} signals in control experiments (data not shown).

Isolation of Primary Mouse Mesothelial Cells—Primary mouse mesothelial cells (prMC) were isolated from 4–6-month-old C57Bl/6J mice according to an established protocol (20) and as applied in our previous study (8). The pelleted cells enriched in mouse mesothelial cells were grown in DMEM/F-12 GlutaMAX medium supplemented with 15% FCS; 0.4 μg/ml hydrocortisone; 10 ng/ml epidermal growth factor; 1% insulin, transferrin, and selenium; 1 mM sodium pyruvate; 0.1 mM β-mercaptoethanol; 1% non-essential amino acids; 1% penicillin-streptomycin; and 2% Mycokill (PAA Laboratories, Paschning, Austria) (21). After a few days (>4 days *in vitro*), cultured cells showed the typical cobblestone-like morphology of mesothelial cells, and cell cultures maintained for ~60 days *in vitro* were used for the measurements.

Plasmids and Lentiviral Infection—For the generation of cell lines stably expressing the Ca^{2+} indicator proteins GCaMP3 (Addgene plasmid 22692 (22)) and mito-CAR-GECO1 (Addgene plasmid 46022 (23)), the lentiviral expression vector pLVTHM (Addgene plasmid 12247 (24)) was used. The GFP cassette in pLVTHM was replaced with cDNAs coding for the respective Ca^{2+} indicator proteins. Briefly, pGCaMP3 was produced in SCS110 dam^- bacteria and digested with AfeI and XbaI, and the fragment was inserted into the PmeI and SpeI sites of the backbone of pLVTHM to produce the final plasmid pLV-GCaMP3. The expression plasmid CMV-mito-CAR-GECO1 was used as template for the production of a DNA fragment coding for mito-CAR-GECO1. The required DNA fragment was synthesized by PCR using the following primers pairs: 5′-TAG CGT TTA AAC GGG CCC TC-3′ and 5′-GAG AAC TAG TTT ACT TCG CTG TCA TCA TTT GTA C-3′. The amplicon was digested with PmeI and SpeI and inserted into the unique sites of the pLVTHM vector to produce the final pLV-mito-CAR-GECO1 plasmid. Calretinin overexpression was achieved by the help of a lentiviral system. Briefly, the GFP cassette in pLVTHM was replaced with the human *CALB2* cDNA coding for full-length calretinin using the previously described expression plasmid RSV-CALB2-neo (25) as template. The DNA fragment coding for full-length calretinin was synthesized by PCR using the primers PmeI-CALB2 (5′-AGT CGT TTA AAC ATG GCT GGC CCG CAG CAG CAG-3′) and SpeI-CALB2 (AGT CAC TAG TTT ACA TGG GGG GCT CGC TGC A-3′). The amplicon was digested with PmeI and SpeI and inserted into the unique sites of the pLVTHM vector to produce the final pLV-CALB2 plasmid. We also generated a lentivirus expressing calretinin (CR) tagged with the enhanced blue fluorescent protein (EBFP) allowing for the easy identification of cells overexpressing EBFP-CR. For this, the pLV-EBFP2-nuc plasmid (Addgene plasmid 36085) and CMV-CALB2-neo were used. The DNA fragment coding for full-length calretinin was synthesized by PCR using the primers XhoI-CALB2 (5′-GAG ACT CGA GTA GCT GGC CCG CAG CAG C-5′) XbaI-CALB2 (5′-GAG ATC TAG ATT ACA TGG GGG GCT CGC TGC A-3′). The amplicon was digested with XhoI and XbaI and inserted into the unique sites of the pLV-EBFP2-nuc vector to produce the final pLV-EBFP2-CR plasmid. As a control plasmid coding for EBFP only (pLV-EBFP2-X), the nuclear localization signal was removed in the plasmid pLV-EBFP2-nuc by deleting an XhoI fragment. All lentiviral plasmids were verified by restriction enzyme digestion and sequencing. Lentivirus was produced by the calcium phosphate transfection method using HEK293T cells and three plasmids: one of the expression plasmids (*e.g.* pLV-GCaMP3 or pLV-mito-CAR-GECO1), the envelope plasmid (pMD2G-VSVG, Addgene plasmid 12259), and the packaging plasmid (psPAX2, Addgene plasmid 12260). Virus-containing supernatants were collected after 48 and 72 h, filtered, aliquoted, and frozen at −80 °C (26). MCU expression was knocked down in prMC expressing GCaMP3 and mito-CAR-GECO1 using

Mission lentiviral transduction particles (Sigma-Aldrich) TRCN0000267404 and TRCN0000265169. Mission transduction particles directed toward human parvalbumin (TRCN000056549) and non-infected cells served as controls. Infected cells were selected using 2 μg/ml puromycin dihydrochloride (Sigma-Aldrich) for 1 week. *MCU* transcript knockdown was verified by qRT-PCR analysis.

qRT-PCR—PrMC were seeded in 6-well plates, and RNA was extracted with 1 ml of PeqGold Trifast (PeqLab, Erlangen, Germany). cDNA synthesis (QuantiTect Reverse Transcription kit, Qiagen, Hombrechtikon, Switzerland) and qRT-PCR (Rotor-Gene SYBR Green PCR kit, Qiagen) were performed following the manufacturers' protocols. Primers were as follows: m*UBC*: forward, 5′-GGA CGC CAC CGT GAA ACA ACT C-3′; reverse, 5′-ACC TCC AGG GTG ATG GTC TTA CCA-3′; m*MCU*: forward, 5′-CTC ACC AGA TGG CGT TCG AGT CG-3′; reverse, 5′-GCG TCG CTG CAT CTT CAT GGC T-3′.

Calcium Imaging—prMC were isolated as described before (27) and grown on collagen-coated glass bottom 35-mm dishes (MatTek Corp., Ashland, MA). The buffer solution (Hepes-buffered saline) used for Ca^{2+} imaging experiments contained 120 mM NaCl; 5.4 mM KCl, 0.8 mM Mg_2Cl, 20 mM Hepes, 1 mM $CaCl_2$, and 10 mM glucose, pH 7.4 (adjusted by NaOH). In the low Ca^{2+} solution, $CaCl_2$ was replaced with an equimolar concentration of NaCl. The drugs (thapsigargin, FCS, and EGTA) were added to the solutions and remained in the solution until the end of the experiments. In some experiments, cells were pretreated either with 250 μM CGP-37157 or with 10 μM Ru-360 for 30 min at 37 °C. Cells were loaded either with 30 μM BAPTA-AM or 30 μM EGTA-AM for 15 min at 37 °C. We used a DMI6000 inverted confocal microscope integrated to a Leica TCS-SP5 work station to examine fluorescence signals indirectly, reporting c_{cyt} or c_{mito}. The following excitation wavelengths were used to illuminate the fluorophores: 488 nm for GCaMP3 and 561 nm for mito-CAR-GECO1. Fluorescence emissions were recorded with a 20× objective and bandpass filters of 505–550 nm for GCaMP3 and 584–683 nm for mito-CAR-GECO1. Fluorescence images for c_{cyt} or c_{mito} measurements were collected every 3 s. Circle-shaped regions of interest (ROIs) were placed inside the cytoplasmic area of cells. The fluorescence values were calculated after background subtraction (fluorescence intensity of regions without cells). Fluorescence intensity values were normalized in each experiment to the averaged basal value preceding the treatment period. A bleaching correction was carried out when the baseline was not stable. LAS-AF (Leica) and Prism5 (GraphPad Software, Inc., San Diego, CA) software were used for data analysis.

ATP Measurements—PrMC were starved in serum-free DMEM supplemented with 1% penicillin-streptomycin for 24 h and distributed into 15 centrifuge tubes (50,000 cells/tube) in 50 μl of Hepes-buffered saline (+Ca^{2+}). 1% FCS was added to 11 tubes, and 6 min later, 100 nM CCCP was added to five tubes. During the experiment, lysis buffer was added into each tube one after another with a delay of 1 min. ATP levels were determined using the ATP bioluminescence assay kit HS II according to the manufacturer's protocol (Roche Applied Science) with a microplate luminometer (PerkinElmer Life Sciences).

Mitochondrial Membrane Potential (ΔΨ) Measurements—Mito-CAR-GECO1-expressing prMC were seeded on glass bottom Petri dishes and incubated with 10 μM Rhodamine 123 for 20 min at room temperature. Cells were washed three times with Hepes-buffered saline (+Ca^{2+}). During the recording using the confocal microscope, a 488-nm excitation wavelength was used to illuminate Rhodamine 123. Fluorescence emissions were recorded with a 20× objective and bandpass filters of 505–550 nm for Rhodamine 123. The distribution of Rhodamine 123 between the mitochondrial matrix and cytosol is proportional to the mitochondrial membrane potential. As the mitochondrial network is distributed within the entire cytoplasmic space, circle-shaped ROIs were randomly assigned to the cytoplasmic region for the fluorescence intensity measurements. The signal intensity is proportional to the amount of Rhodamine 123 dye incorporated by mitochondria in this ROI. For the normalization and thus the measurement of Rhodamine 123 released by mitochondria, an ROI within the nuclear region not containing mitochondria was selected, and the fluorescence intensity in this ROI was determined. The relative (rel.) ΔΨ was calculated according to the following equation.

$$\Delta\psi_{rel} = \frac{F_{mito}}{F_{nucl}} \qquad \text{(Eq. 1)}$$

where F_{mito} and F_{nucl} are the fluorescence intensity of Rhodamine 123 in the mitochondrial and nuclear regions, respectively. The mitochondrial membrane potential was additionally measured with tetramethylrhodamine methyl ester. For these measurements, cells were preincubated with 50 nM tetramethylrhodamine methyl ester for 30 min.

Estimation of the Intracellular Calretinin Concentration by Western Blot Analysis—Protein samples were isolated from cultured prMC. Cells were grown in 25-cm^2 flasks and harvested at near confluence. Total proteins were extracted with ice-cold radioimmune precipitation assay buffer. Serial dilutions of protein extracts (50, 5, 0.5, and 0.005 μg) from each cell culture sample as well as 40 ng of purified human recombinant calretinin were loaded onto SDS-polyacrylamide gels (12.5%). After separation, proteins were transferred onto nitrocellulose membranes (Bio-Rad) and incubated overnight at 4 °C with the calretinin-specific antibody CR7699/4 (Swant, Marly, Switzerland) at a dilution of 1:10,000. Rabbit secondary antibody linked to horseradish peroxidase (Sigma-Aldrich) was diluted at 1:10,000, and membranes were incubated for 4 h. For the detection, the chemiluminescent reagent Luminata Classico Forte (EMD Millipore Corp., Billerica, MA) was used. Chemiluminescent and normal illumination digital images were recorded on a system from Cell Biosciences (Santa Clara, CA). Area densities of calretinin bands were measured with ImageJ software. From the density curves, the cell protein concentration corresponding to 40 ng of calretinin was determined. This allowed determination of calretinin or more precisely that of the fusion protein EBFP-calretinin content in μg/mg of total protein. Based on previous estimation of a protein concentration of about 0.2 g/ml (28) in mammalian cells, the intracellular concentration of EBFP-calretinin was estimated.

Frequency Determination and Amplitude Scan—Computerized peak recognition for frequency and amplitude analyses was realized via the Microsoft Excel 2010 environment as described before (8); normalized recordings from >30 oscillating prMC were evaluated. The oscillation frequency as well as the average amplitude was determined for three time windows: 1–5, 5–9, and 9–13 min after serum administration.

Mathematical Simulation—To build the mathematical model, we considered four compartments: the extracellular space, cytoplasm, mitochondrial matrix, and ER lumen (Fig. 1). A fifth element placed within the cytoplasm in some simulations was the presence of a Ca^{2+} buffer. Membrane junctions between the ER and the plasma membrane ensured that the functional unit components (Ca^{2+} channels and pumps) are concentrated spatially in a very small space (29). Similarly close contacts were also assumed to exist between mitochondria and ER (30). One oscillatory unit represents an inositol trisphosphate receptor ($InsP_3R$) cluster and its surrounding. We presumed that changes in c_{cyt}, c_{ER}, and c_{mito} of the entire cell were similar to that of individual units, *i.e.* spatially homogenous. In our view, this simplification is acceptable because the oscillations are slow and the cell size is small. In this case, the spatial diffusion of Ca^{2+} rapidly equilibrates the putative spatial differences and thus synchronizes the functions of individual functional units (31). In a cell with a 10-μm diameter, the diffusion is estimated to equilibrate spatial heterogeneity in c_{cyt} in less than 0.1 s (32). However, because Ca^{2+} waves not only depend on Ca^{2+} diffusion but also on the action of Ca^{2+} pumps and channels, the Ca^{2+} wave is ~10 times slower (33). Although our model is a minimal deterministic point model and cannot produce the stochastic and spatial phenomena of the Ca^{2+} oscillations, it is a useful tool to illuminate the observed characteristics of the mitochondrial Ca^{2+} handling. Our aim was to build the most simple model still able to produce the experimentally observed phenomena.

Ca^{2+} transports across the plasma membrane were defined as J_{IN} and J_{EFF}, and the transports across the ER membrane were termed J_{SERCA} and J_{EREFF}, respectively. J_{IN} includes Ca^{2+} channels in the plasma membrane, *e.g.* voltage-gated Ca^{2+} channels, transient receptor potential channels, store-operated channels, P2X purinoreceptors, hyperpolarization-activated cyclic nucleotide-gated channels, etc. The J_{EFF} represents the pumps involved in Ca^{2+} extrusion, plasma membrane Ca^{2+}-ATPases and Na^+/Ca^{2+} exchangers. The SERCA pumps transport Ca^{2+} from the cytoplasm to the ER, whereas the J_{EREFF} represents the ER channels involved in emptying the ER, ryanodine receptor and $InsP_3R$. The function of the mitochondrial exchangers (J_{MEXC}) and the mitochondrial calcium uniporter (J_{MCU}) are responsible for the Ca^{2+} transport across the mitochondrial inner membrane (see Fig. 1).

We denote by c_{cyt} the Ca^{2+} concentration (in nM) in the cytosol and by c_{ER} that in the lumen of the ER. Mitochondrial matrix free concentration is denoted by c_{mito}. The equations for the model are as follows.

$$\frac{dc_{cyt}}{dt} = J_{IN} - J_{EFF} - J_{SERCA} + J_{EREFF} + J_{ERLEAK} - J_{MCU} + J_{MEXC} \quad \text{(Eq. 2)}$$

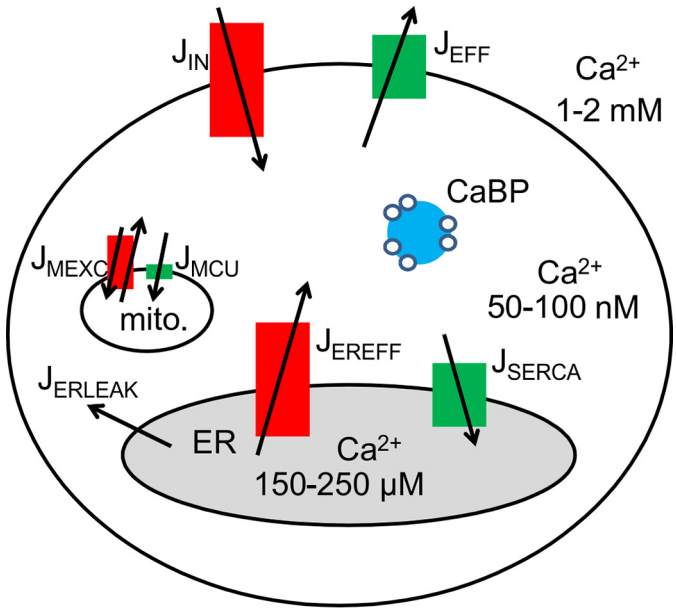

FIGURE 1. **Schematic model of cellular compartments and Ca^{2+} toolkit components implicated in Ca^{2+} oscillations in prMC.** The plasma membrane contains components responsible for Ca^{2+} influx (J_{IN}) and efflux (J_{EFF}). The dominant intracellular Ca^{2+} release (J_{EREFF}) and uptake (J_{SERCA}) systems are localized in ER membranes. A small constant leak (J_{ERLEAK}) occurs independently of Ca^{2+} channels. The functions of the mitochondrial Ca^{2+} exchangers (Na^+/Ca^{2+} exchanger and H^+/Ca^{2+} exchanger) (J_{MEXC}) and the mitochondrial calcium uniporter (J_{MCU}) are responsible for the Ca^{2+} transport across the mitochondrial inner membrane; intracellular Ca^{2+} buffers (*CaBP*) such as calretinin acting as a transient cytosolic Ca^{2+} store/source modulate temporal aspects of c_{cyt} and consequently affect Ca^{2+} fluxes across all membranes (plasma membrane, ER, and mitochondria (*mito.*)).

$$\frac{dc_{ER}}{dt} = \gamma(J_{SERCA} - J_{EREFF} - J_{ERLEAK}) \quad \text{(Eq. 3)}$$

$$\frac{dc_{mito}}{dt} = \rho(J_{MCU} - J_{MEXC}) \quad \text{(Eq. 4)}$$

where J_{IN} is the flux of Ca^{2+} ions entering the cell, J_{EFF} is the Ca^{2+} flux pumped out of the cell, J_{SERCA} denotes the Ca^{2+} flux pumped from the cytosol to ER, J_{EREFF} is the flux of Ca^{2+} passing from the ER to the cytosol, J_{MCU} denotes the function of MCU, J_{MEXC} displays the function of mitochondrial Ca^{2+} exchangers (mitochondrial Na^+/Ca^{2+} and H^+/Ca^{2+} exchangers), and finally J_{ERLEAK} represents a small flux of Ca^{2+} diffusing from the ER to the cytosol (all values in nM/s).

The constant γ is the ratio between the changes in c_{cyt} and c_{ER} caused by the same quantity of Ca^{2+} ions transported through the ER membrane. This value is derived from the difference in the effective volume of the ER lumen and the cytoplasm and from the different fraction of free and protein-bound Ca^{2+} in these compartments (34). The value of the γ parameter was estimated experimentally (8).

The quantity of Ca^{2+} pumped out of the cell through the plasma membrane increases as a function of the Ca^{2+} concentration in the cytosol. The Na^+/Ca^{2+} exchangers have low Ca^{2+} affinity but high capacity for Ca^{2+} transport, whereas the plasma membrane Ca^{2+}-ATPases have a high Ca^{2+} affinity but a low transport capacity. Although the individual components of extrusion systems are usually modeled by Hill equations (35), the overall flux can be simulated by a simple linear equation (36)

based on the experimental results of Herrington *et al.* (37).

$$J_{\mathrm{EFF}} = \begin{cases} 0, r_{e1}c_{\mathrm{cyt}} - r_{e2} \le 0 \\ r_{e1}c_{\mathrm{cyt}} - r_{e2}, r_{e1}c_{\mathrm{cyt}} - r_{e2} > 0 \end{cases} \quad \text{(Eq. 5)}$$

where r_{e1} and r_{e2} are two positive constants.

SERCAs pump the Ca^{2+} ions from the cytosol to the ER. The quantity of the transported Ca^{2+} ions depends on c_{cyt} levels. We assume a linear relationship because the ER influx is also composed of different SERCA pumps with different K_d values (38). Nevertheless, our model can also work when J_{EFF} and/or J_{SERCA} is simulated with the conventional Hill equations.

$$J_{\mathrm{SERCA}} = \begin{cases} 0, r_{s1}c_{\mathrm{cyt}} - r_{s2} \le 0 \\ r_{s1}c_{\mathrm{cyt}} - r_{s2}, r_{s1}c_{\mathrm{cyt}} - r_{s2} > 0 \end{cases} \quad \text{(Eq. 6)}$$

where r_{s1} and r_{s2} are two positive constants.

Ca^{2+} ions are released from the ER to the cytosol through $InsP_3R$ and ryanodine receptor. Because we found experimentally that ryanodine receptor does not play a role in serum-induced oscillations in mesothelial cells (8) similarly to other non-excitable cells (39), we focused on $InsP_3R$. In our model, $InsP_3R$ is influenced both by c_{cyt} and by c_{ER} but without an allosteric regulation between the two. $InsP_3R$ has Ca^{2+} binding sites not only on the cytoplasmic side but also on the luminal side (40). Experimental data show that an increase in inositol trisphosphate ($InsP_3$) concentration causes a significant Ca^{2+} release from the ER in the absence of cytosolic Ca^{2+} ($c_{\mathrm{cyt}} = 0$) (41). Moreover, the effects of luminal Ca^{2+} do not affect the cytosolic binding sites (42, 43). Therefore we modeled $InsP_3R$ function as the sum of two individual contributions.

$$J_{\mathrm{EREFF}} = \begin{cases} 0, J_{\mathrm{cytdep}} + J_{\mathrm{ERdep}} \le 0 \\ J_{\mathrm{cytdep}} + J_{\mathrm{ERdep}}, J_{\mathrm{cytdep}} + J_{\mathrm{ERdep}} > 0 \end{cases} \quad \text{(Eq. 7)}$$

where

$$J_{\mathrm{cytdep}} = r_{i,\max}\exp\left(-\frac{(\log(c_{\mathrm{cyt}}) - \mu)^2}{\sigma^2}\right) \quad \text{(Eq. 8)}$$

and

$$J_{\mathrm{ERdep}} = r_{i1}\log(c_{\mathrm{ER}}) - r_{i2} \quad \text{(Eq. 9)}$$

with positive constants σ and r_{i1}.

We introduced the dependence of $InsP_3R$ on the [$InsP_3$], which has an influence both on J_{cytdep} and on J_{ERdep}. According to the experimental data from several studies (44–46), elevating c_{IP3} mainly changes the mean and the maximum (μ and $r_{i,\max}$) of the bell-shaped curve of c_{cyt} dependence. Nevertheless, based on the experimental data presented (47, 48), elevating c_{IP3} also has an effect on the loading of the ER. Increased c_{IP3} reduces the amount of the stored Ca^{2+} ions. We simulated this effect by changing the r_{i2} parameter.

$$\mu = \mu_{\min} + (\mu_{\max} - \mu_{\min})\frac{K_b}{K_b + c_{\mathrm{IP3}}} \quad \text{(Eq. 10)}$$

$$r_{i,\max} = r_{\mathrm{im,min}} + (r_{\mathrm{im,max}} - r_{\mathrm{im,min}})\frac{K_b}{K_b + c_{\mathrm{IP3}}} \quad \text{(Eq. 11)}$$

$$r_{i2} = r_{i2,\min} + (r_{i2,\max} - r_{i2,\min})\frac{K_b}{K_b + c_{\mathrm{IP3}}} \quad \text{(Eq. 12)}$$

where K_b is the half-saturation constant of $InsP_3R$ for $InsP_3$ and c_{IP3} represents the $InsP_3R$ sensitivity to the inositol trisphosphate molecule, which was taken equal to inositol trisphosphate concentration in μM. $\mu_{\max}$, $\mu_{\min}$, $r_{\mathrm{im,min}}$, $r_{\mathrm{im,max}}$, $r_{i2,\min}$, and $r_{i2,\max}$ are positive constants. The parameter J_{ERLEAK} accounts for a Ca^{2+} flux from the ER to the cytoplasm independently of known Ca^{2+} channels, and this parameter is assumed to represent a small constant value (49).

$$J_{\mathrm{ERLEAK}} = \beta \quad \text{(Eq. 13)}$$

The outer membrane of mitochondria is freely permeable for Ca^{2+} ions, but the inner mitochondrial membrane provides a barrier. The constant ρ is the ratio between the changes in c_{cyt} and c_{ER} caused by the same quantity of Ca^{2+} ions transported through the mitochondrial inner membrane. This value is derived from the difference in the effective volume of the mitochondrial matrix and the cytoplasm and from the different fraction of free and protein-bound Ca^{2+} in these compartments.

There is a fast Ca^{2+} influx into the mitochondria matrix if c_{cyt} reaches a certain value. This fast influx is attributable to the function of MCU. We used Hill equations with a very high Hill coefficient as was done in the work of Marhl *et al.* (50). For simplicity, we did not take into account the changes in mitochondrial transmembrane potential and in mitochondrial volume during the Ca^{2+} oscillations in line with Marhl *et al.* (50), but we have to consider it during a protonophore treatment. The passage of calcium ions through the MCU requires the large membrane potential difference generated by the action of the electron transport chain (51).

$$J_{\mathrm{MCU}} = \Delta\Psi \times r_{\psi} \times v_{\mathrm{MCU,MAX}}\frac{{c_{\mathrm{cyt}}}^{H}}{{K_{d,\mathrm{MCU}}}^{H} + {c_{\mathrm{cyt}}}^{H}} \quad \text{(Eq. 14)}$$

where r_{Ψ} and $\nu_{\mathrm{MCU,max}}$ are positive constants, $K_{d,\mathrm{MCU}}$ is the dissociation constant of MCU for Ca^{2+} ions, and H is the Hill coefficient. In our model, J_{MCU} has a constant basal activity. That ensures that mitochondria can store a small amount of Ca^{2+} ions, which are released into the cytoplasm immediately after the collapse of the mitochondrial membrane potential. Higher $\Delta\Psi$ means increased Ca^{2+} uptake but slower mitochondrial Ca^{2+} release.

To simulate the function of mitochondrial exchangers (Na^+/Ca^{2+} and H^+/Ca^{2+} exchangers), we consider that both will transport Ca^{2+} ions with a low velocity when there is a concentration gradient between the two sides of the mitochondrial inner membrane. For the simplicity, we neglected the changes in sodium and proton concentrations during the Ca^{2+} oscillations. Depending on the calcium concentration gradient, the exchangers can work in both directions.

$$J_{\mathrm{MEXC}} = \left(\frac{c_{\mathrm{mito}}}{\rho \times c_{\mathrm{cyt}}} - 1\right) \times (\Delta\Psi \times r_{\mathrm{m1}} - r_{\mathrm{m2}}) \quad \text{(Eq. 15)}$$

where r_{m1} and r_{m2} are positive constants.

The Ca^{2+} influx across the plasma membrane is composed of passive leakage and the agonist-activated fluxes: the capacitive

(store-operated channel-dependent) and the non-capacitive (arachidonate- or diacylglycerol-regulated) Ca^{2+} influx (52). We simulated the changes in J_{IN} starting from the beginning of the administration of serum (t_1) using the following equations.

$$J_{IN} = 0.1\text{nM/s if } t < t_1 \text{(only passive leakage)} \quad \text{(Eq. 16)}$$

$$J_{IN} = r_{IN,MAX}\frac{(t - t_1)}{K_{IN,1} + (t - t_1)} \text{ if } t_1 \le t \le t_2 \quad \text{(Eq. 17)}$$

$$J_{IN} = (r_{IN,MAX} - r_{IN,p}) \times \exp(-K_{IN,2}(t - t_2)) + r_{IN,p} \text{ if } t > t_2 \quad \text{(Eq. 18)}$$

We simulated the changes in c_{IP3} from the beginning of the administration of serum (t_1) with the following equations. The resting c_{IP3} was set to 15 nM (53).

$$c_{IP3} = 0.015 \text{ if } t < t_1 \quad \text{(Eq. 19)}$$

$$c_{IP3} = c_{IP3,MAX}\frac{(t - t_1)}{K_{IP3} + (t - t_1)} \text{ if } t \ge t_1 \quad \text{(Eq. 20)}$$

To simulate the effect of calretinin, we neglected its fast kinetics. Because this protein is considered as a fast Ca^{2+} buffer (54), calretinin reaches the Ca^{2+} steady state in a few milliseconds, which is much faster than our observed Ca^{2+} changes lasting for a few seconds. The fast kinetics of calretinin plays an important role at the mouth of voltage-gated Ca^{2+} channels in excitable cells (55) where fast and large changes in Ca^{2+} concentrations are expected.

$$\frac{dc_{cyt}}{dt} = J_{IN} - J_{EFF} - J_{SERCA} + J_{EREFF} + J_{ERLEAK} - J_{MCU} + J_{MEXC} + c_{CR}\nu \quad \text{(Eq. 21)}$$

where c_{CR} is the concentration of calretinin in the cytoplasm and ν is the average number of the Ca^{2+} binding sites of calretinin occupied by Ca^{2+}. Calretinin has four high affinity Ca^{2+} binding sites and one low affinity binding site. The binding kinetics of the Ca^{2+} binding sites were simulated with Hill equations.

$$\nu = 4 \times \frac{c_{cyt}^{\ h}}{K_{d1}^{\ h} + c_{cyt}^{\ h}} + \frac{c_{cyt}}{K_{d2} + c_{cyt}} \quad \text{(Eq. 22)}$$

where K_{d1} is the dissociation constant for the high affinity Ca^{2+} binding sites, K_{d2} is the dissociation constant for low affinity Ca^{2+} binding site, and h is the Hill coefficient for the high affinity binding sites. Among the high affinity Ca^{2+} binding sites, there is a positive cooperativity ($h > 1$). The values for the parameters came from the study of Faas *et al.* (54).

The values of each parameter are listed in Table 1. The initial values of parameters are derived either from our experiments in primary mesothelial cells or from fitting to experimental data previously reported in the above mentioned articles. The presented values are the result of the sequential fitting of the initial values to our *in situ* recordings. All computations of the model were implemented in the Microsoft Excel 2010 environment. The model system was discretized with a temporal resolution of 0.1 s (supplemental Excel document). There were no significant differences in the solution of the differential equations if we increased the temporal resolution (not shown). For visualization, Prism5 (GraphPad Software, Inc.) software was used.

TABLE 1
Parameters used for the modeling

Equation to determine	Parameter name	Value
	γ	450
	ρ	4
J_{EFF} (Equation 5)[a]	r_{e1}	0.17/s
	r_{e2}	18.8 nM/s
J_{SERCA} (Equation 6)[a]	r_{s1}	0.27/s
	r_{s2}	22 nM/s
J_{EREFF} (Equations 8 and 9)	σ	0.14142 nM
	r_{i1}	1300/s
μ (Equation 10)	μ_{min}	2.4 nM
	μ_{max}	2.18 nM
	K_b	2 μM
$r_{i,max}$ (Equation 11)	$r_{im,min}$	821.3 nM/s
	$r_{im,max}$	24.3 nM/s
	K_b	2 μM
r_{i2} (Equation 12)	$r_{i2,min}$	6352 nM/s
	$r_{i2,max}$	7042 nM/s
	K_b	2 μM
J_{ERLEAK} (Equation 13)	β	2.5 nM/s
	c_{ER} (initial)	260 μM
	c_{cyt} (initial)	110 nM
	$\Delta\Psi$ (initial)	180 mV
J_{MCU} (Equation 14)	r_{Ψ}	0.005555/mV
	$\nu_{MCU,MAX}$	5 nM/s
	$K_{d,MCU}$	208 nM
	H	7.4
J_{MEXC} (Equation 15)	r_{m1}	−0.01251/mV
	r_{m2}	2.295
ν (Equation 22)	K_{d1}	2.5 μM
	K_{d2}	53 μM
	h	2.4
J_{IN} (Equations 16, 17, and 18)	t_1	60 s
	t_2	72 s
	$r_{IN,MAX}$	5 nM/s
	$K_{IN,1}$	0.01 s
	$r_{IN,p}$	1.05 nM/s
	$K_{IN,2}$	2 s
c_{IP3} (Equations 19 and 20)	$c_{IP3,MAX}$	1.8 μM
	K_{IP3}	0.1 μM

[a] Alternatively, the J_{EFF} and J_{SERCA} can be simulated conventionally with a Hill equation with the following parameters: V_{max}, 260 and 170 nM/s; K_d, 460 and 480 nM; and Hill coefficients, 3.5 and 2.4, respectively.

Results

Characterizing Ca^{2+} Fluctuations in Mitochondria of Primary Mouse Mesothelial Cells—In the absence of serum, prMC did not show Ca^{2+} oscillations as reported before (8). However, in a small fraction of cells (2–3%), isolated arrhythmic mitochondrial increases in c_{mito} were present without detectable changes in c_{cyt} (Fig. 2*A*). The addition of 1% FCS to the cell culture medium containing prMC that were grown in the absence of serum for 24 h resulted in a sudden rise of c_{cyt} lasting, on average, for ~40 s followed by Ca^{2+} oscillations (Fig. 2, *B–D*). The percentage of prMC responding to serum readministration with Ca^{2+} oscillations was in the order of 70%. Non-oscillatory cells showed only an initial single Ca^{2+} transient or a so-called peak-plateau response (53). A wide range of different oscillatory patterns in c_{cyt} was present in a supposedly homogenous population of mesothelial cells. Most cells displayed long period (>10 min) baseline spiking oscillations with various frequencies of one spike per 3 min (Fig. 2*B*) up to 10 per min (Fig. 2*D*); also maximal spike amplitudes varied between individual cells. The baseline spiking oscillations represent discrete Ca^{2+} transients starting from a constant basal c_{cyt} level (Fig. 2, *B* and *C*). Sinusoidal oscillation is a term for a continuous fluctuation

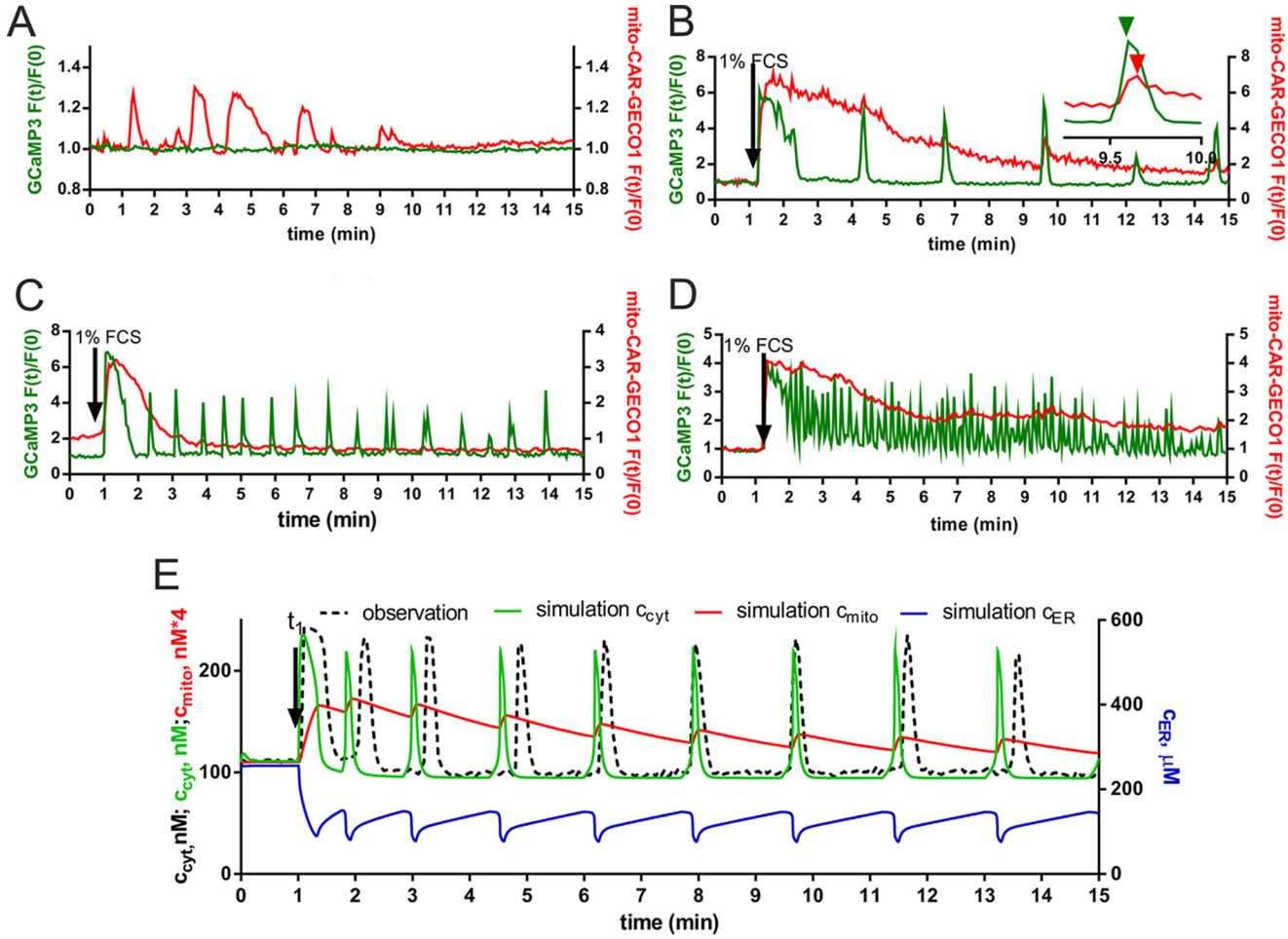

FIGURE 2. **Ca^{2+} oscillations in c_{cyt}, c_{ER}, and c_{mito} in prMC.** *A*, a representative recording shows spontaneous mitochondrial Ca^{2+} transients (*red* trace) in a resting cell without changes in c_{cyt} (*green* trace). *B–D*, single cell fluorescence recordings derived from time lapse videos show the simultaneous changes in c_{cyt} (*green* traces) and c_{mito} (*red* traces) after serum readministration. Despite the different oscillatory frequencies (increasing from *B* to *D*) in c_{cyt}, the traces for c_{mito} were very similar in all three recordings: a fast initial rise followed by a quasiexponential decay with varying kinetics. The small *inset* in *A* shows (at an expanded time scale) that small fluctuations (short rises in c_{mito}) coincide with c_{cyt} spikes. The peak in c_{mito} is slightly delayed in comparison with the peak in c_{cyt}. *E*, an experimental recording (*black dashed line*) in prMC showing low frequency oscillations was selected for the fitting. The model shows the changes in c_{cyt} (*green* trace), c_{mito} (*red* trace), and c_{ER} (*blue* trace). The parameters and equations are presented in the supplemental Excel document. The changes in c_{mito} consist of an initial rise after FCS administration followed by a slow return to basal levels. Each Ca^{2+} spike in c_{cyt} results in a small hump in c_{mito} reaching its relative maximum with a small delay compared with the maximum in c_{cyt}. Original recordings for c_{ER} in prMC were previously presented (8); they show sawtooth-like waves at a semidepleted ER state during Ca^{2+} oscillations as shown in our model here (*blue* trace).

in c_{cyt} starting from a c_{cyt} value that is higher than the resting (basal) c_{cyt} (Fig. 2*D*). Most probably, sinusoidal oscillations are the result of high frequency overlapping baseline spiking oscillations (56). In prMC maintained in cell culture medium for longer periods (>10 passages), the percentage of the cells showing sinusoidal oscillations was increased as exemplified in Fig. 2*D*. However, the percentage of cells showing oscillatory activity was rather low at higher passages (~20–40% at passages >10). The average frequency of the baseline spiking oscillations was found to be 15, 13, and 13 mHz in the following time segments: 1–5, 5–9, and 9–13 min after serum administration, respectively. The average amplitude of spikes (-fold increase in GCaMP3 fluorescence intensity) was found to be 2.66, 2.53, and 2.53 in the above mentioned time segments. By using two Ca^{2+} indicators targeted to either the mitochondrial matrix (mito-CAR-GECO1) or the cytoplasm (GCaMP3), we simultaneously monitored changes in c_{mito} and c_{cyt}, respectively. The initial serum-induced rise in c_{cyt} was paralleled by a rapid rise in c_{mito} that reached the peak value within 30 s after the addition of 1% FCS (Fig. 2, *B–D*); from then on, c_{mito} decreased continuously until it reached its initial basal value, generally within the time span of 15 min monitored in most experiments. High frequency oscillations in c_{cyt} resulted in continuous elevation in c_{mito} (Fig. 2*D*). The rate of decay in c_{mito} was also rather variable between cells, and oscillations in c_{cyt} did not stop when c_{mito} had reached its basal levels. In some cells during the decreasing phase in c_{mito}, small fluctuations (short rises in c_{mito}) coincided with the c_{cyt} spikes but with a small delay (*e.g.* shown in Fig. 2*B*, *inset*). For the modeling, we took into account our previous results where basal and maximal c_{cyt} values during Ca^{2+} spikes in prMC were found to be 100 and 200–300 nM, respectively (8). Similarly, the values for the resting c_{ER} were taken as 150–250 μM, and the values after serum readministration were taken as 100–150 μM (8). The pattern of c_{ER} changes is best described as a sawtooth wave (8). These data were incorporated to build the mathematical model where Ca^{2+} concentrations in all compartments (c_{cyt}, c_{mito}, and c_{ER}) were calculated and fitted to one c_{cyt} recording (Fig. 2*E*). The model accurately recapitulated the

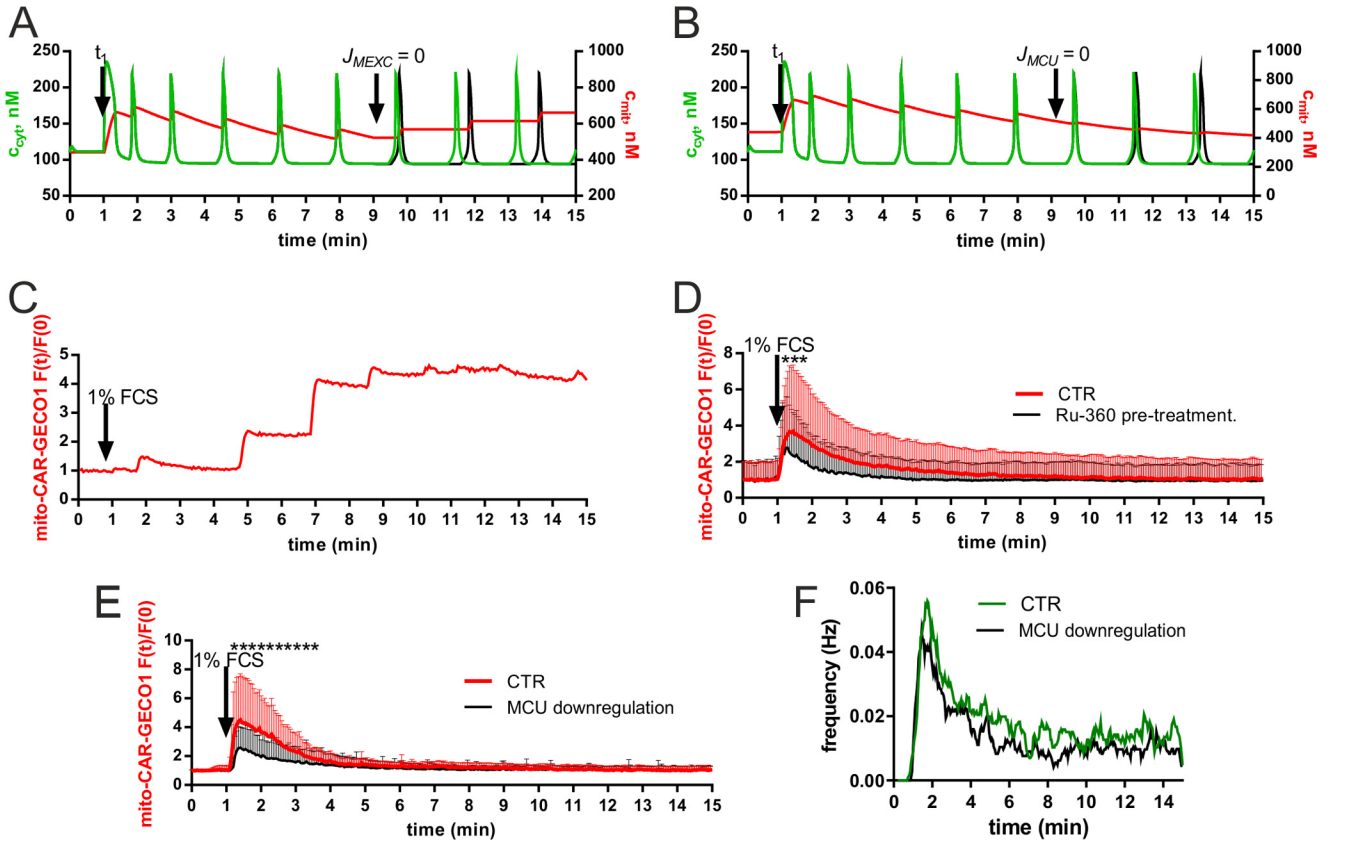

FIGURE 3. **Modulation of mitochondrial Ca^{2+} transport in prMC.** *A*, in the simulation, blocking of the mitochondrial Na^+/Ca^{2+} exchanger activity (J_{MEXC} = 0) at 9 min predicts a staircase-like increase in c_{mito} (*red* trace) following each Ca^{2+} spike, and the oscillation frequency is expected to decrease (*black* trace) compared with the unperturbed situation (*green* trace). *B*, in the simulation, MCU activity was stopped (J_{MCU} = 0) at 9 min. This resulted in the absence of humps in c_{mito} following the Ca^{2+} spikes and a decrease in oscillation frequency (compare *green* trace for c_{cyt} (control conditions) with *black* trace) when J_{MCU} = 0. *C*, a representative recording of c_{mito}, obtained in prMC pretreated for 30 min with CGP-37157 (50 μM), which blocked mitochondrial Ca^{2+} release, is depicted. As predicted by the model (*A*), a staircase-like increase in c_{mito} was observed after each cytosolic Ca^{2+} spike. *D*, reduction in mitochondrial Ca^{2+} uptake was observed in oscillatory prMC pretreated with 10 μM Ru-360; data are mean + S.D. from 10 cells each. *Asterisks* indicate significance at $p < 0.05$. *E*, reduction in mitochondrial Ca^{2+} uptake was observed in oscillatory prMC with down-regulated MCU; data are mean + S.D. from 20 cells each. *Asterisks* indicate significance at $p < 0.05$. *F*, frequency scan analyses of control (*CTR*) cells (*green* trace) and shMCU-treated (*black* trace) cells ($n \geq 50$ oscillating cells for both conditions). In all time windows, the frequency was lower in cells where MCU had been down-regulated. *Error bars* represent S.D.

experimental findings, in particular with respect to c_{mito}, which had not been modeled in our previous study (8). The pattern in c_{mito} is best described as a sudden rise after serum readministration followed by a rather smooth decay phase with small humps (increases in c_{mito}) as the result of the oscillatory Ca^{2+} spikes.

Modulation of Mitochondrial Ca^{2+} Transport Mechanisms Affects Ca^{2+} Oscillations—In the next series of experiments and modeling simulations, we investigated how altering mitochondrial function, mostly in relation to Ca^{2+} handling, affects c_{cyt} oscillations. The simulation showed that inhibition of the mitochondrial Ca^{2+} release (J_{MEXC}) or mitochondrial Ca^{2+} uptake (J_{MCU}) during Ca^{2+} oscillations decreased the oscillation frequency (Fig. 3, *A* and *B*). The experimental verification of our predictions was hampered by the absence of pharmacological mitochondrially targeted compounds that immediately reach the mitochondrial inner membrane when added to the recording solution. Briefly, after serum readministration, the addition of CGP-37157 (50 μM), a nonspecific blocker of the mitochondrial Na^+/Ca^{2+} exchanger, had no effect on the patterns of Ca^{2+} oscillations in either c_{cyt} or c_{mito} (data not shown). However, some cells pretreated with CGP-37157 for 30 min displayed stairlike increases in c_{mito} (Fig. 3*C*), an effect predicted from our model (see Fig. 3*A*, *right part* (c_{mito})). Ruthenium compounds, *e.g.* ruthenium red and Ru-360, are potent and effective blockers of MCU in isolated mitochondria, but their usefulness for intact cells is limited by their poor membrane permeability and selectivity (57). Pretreatment of cells with 10 μM Ru-360 reduced the average oscillation frequency (approximately a 30% decrease during each time segment) and the initial mitochondrial Ca^{2+} uptake (Fig. 3*D*). However, it is currently still unclear whether in intact cells Ru-360 acts uniquely by the inhibition of the mitochondrial Ca^{2+} uptake or additionally by the inhibition of the extracellular Ca^{2+} influx. Therefore, we also used a molecular approach, *i.e.* down-regulation of MCU by shRNA to decrease the mitochondrial Ca^{2+} uptake. The down-regulation of *MCU* mRNA levels by 60–90% as determined by qRT-PCR resulted in a 40–60% decrease in the initial mitochondrial Ca^{2+} uptake (Fig. 3*E*). This led to an ~20% reduction in the c_{cyt} oscillation frequency calculated by frequency scan analysis (Fig. 3*F*) in line with the predictions from our model (Fig. 3*B*). In all time windows (bins of 3 s), the oscillation frequency was lower in prMC where MCU had been down-regulated. Thus, both approaches (Ru-360 and shMCU)

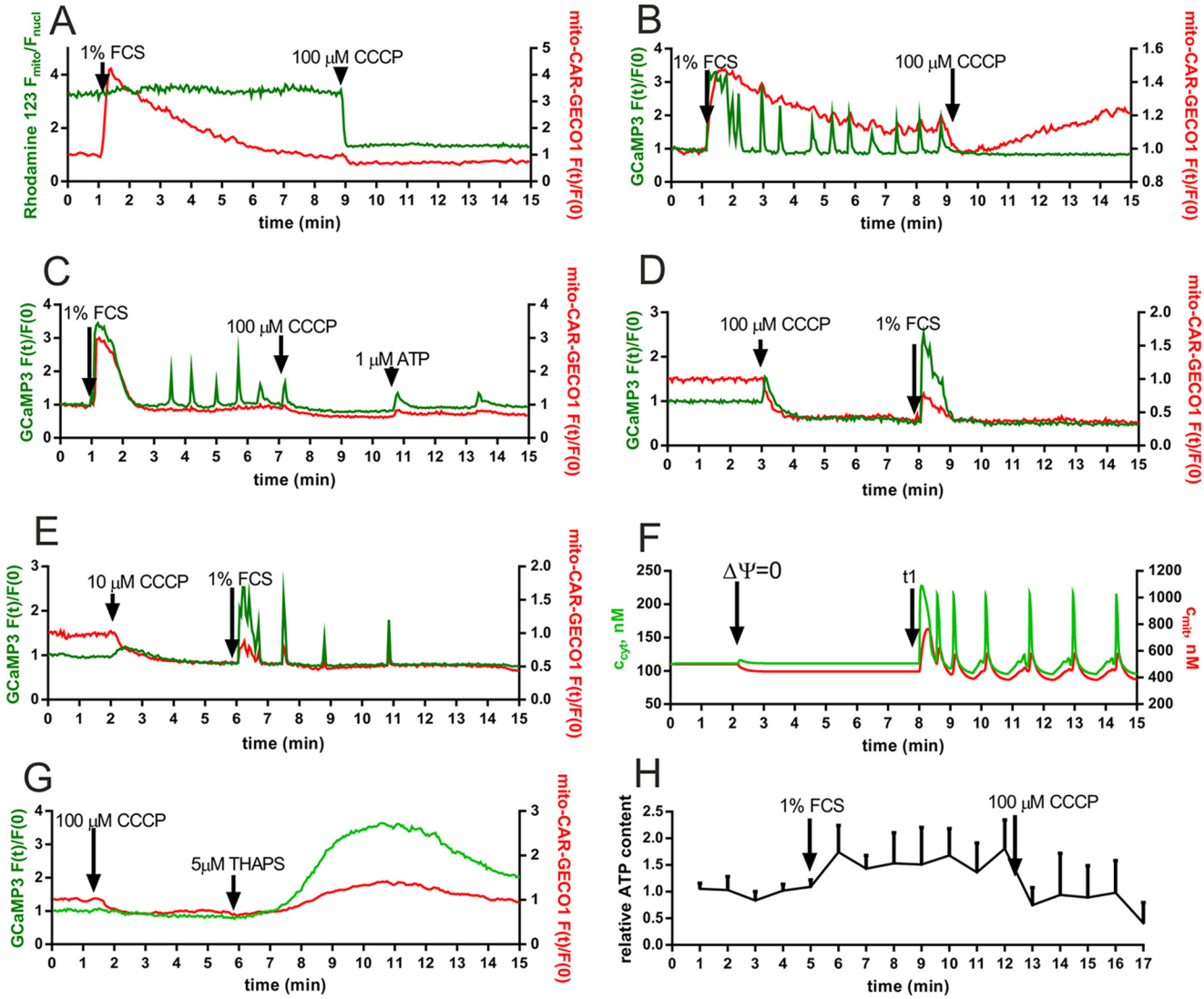

FIGURE 4. **Effect of the proton uncoupler CCCP on Ca^{2+} oscillations.** *A*, serum addition to prMC led to a rapid rise in c_{mito} (*red* trace) followed by a gradual decay. Addition of CCCP (100 μM) resulted in a rapid collapse of the membrane potential as evidenced by measuring Rhodamine 123 fluorescence signals (*green* trace). As the result of CCCP application, c_{mito} immediately returned to basal levels because the slightly elevated c_{mito} level (compared with the c_{cyt} level) could not be maintained when the driving force for mitochondrial Ca^{2+} uptake was eliminated. *B–H*, the role of the membrane potential and ATP treatment was investigated in greater detail, and one representative recording for each experimental condition is depicted. *B*, the addition of CCCP (100 μM) at $t = 9$ min blocked the serum-induced cytosolic Ca^{2+} oscillations. CCCP treatment led to a rapid fall in c_{mito}; in some cells, a slow increase in c_{mito} occurred afterward (*B*), whereas in others, c_{mito} remained low (not shown). *C*, administration of ATP (1 μM) reestablished the CCCP-inhibited Ca^{2+} oscillations in some cells. *D*, addition of CCCP (100 μM) prior to serum readministration lowered the resting c_{mito} (also reflected by the simultaneous small increase in c_{cyt}). However, from then onward, c_{cyt} dropped to levels lower then the basal c_{cyt} before CCCP treatment. The serum readministration at $t = 8$ min evoked only a single Ca^{2+} transient. *E*, at a lower CCCP concentration (10 μM), addition of 1% FCS at $t = 6$ min resulted in elevations in c_{cyt} and c_{mito} followed by a few oscillations in c_{cyt}. The small amount of Ca^{2+} ions taken up by mitochondria (*red* trace) during Ca^{2+} spikes (*green* trace) was released back to the cytosol almost immediately. *F*, in this simulation experiment, the mitochondrial membrane potential was switched off ($\Delta\Psi = 0$) at $t = 3$ min; this resulted in a slight increase in c_{cyt} and a decrease in c_{mito} to values lower than basal c_{mito} as observed experimentally in *D* and *E*. Serum readministration evoked oscillatory activity in c_{cyt} and c_{mito}. *G*, after the CCCP-induced collapse in $\Delta\Psi$, ER Ca^{2+} release by thapsigargin (5 μM) resulted in mitochondrial Ca^{2+} uptake (*red* trace) independent of $\Delta\Psi$. A representative recording displays the simultaneous changes in c_{mito} (*red*) and c_{cyt} (*green*). *H*, during FCS-induced Ca^{2+} oscillations, ATP levels in prMC were increased but dropped quickly after CCCP administration. The panel shows the mean + S.D. of three independent experiments. *Error bars* represent S.D.

underscore the importance of mitochondria in Ca^{2+} oscillations.

CCCP is an inhibitor of oxidative phosphorylation by acting as a protonophore; *i.e.* it allows H^+ to cross the inner mitochondrial membrane, resulting in the collapse of $\Delta\Psi$. During Ca^{2+} oscillations, $\Delta\Psi$ was slightly increased (more negative), but it collapsed immediately after CCCP (100 μM) treatment (Fig. 4*A*). The collapse of the membrane potential after addition of 10 or 100 μM CCCP was also confirmed by using the tetramethylrhodamine methyl ester indicator dye (data not shown). When applied during Ca^{2+} oscillations resulting from serum readministration, CCCP blocked Ca^{2+} oscillations at 100 μM but not at 10 μM (data not shown). An immediate drop in c_{mito} was observed after CCCP treatment (Fig. 4*B*) followed by a continuous elevation in c_{mito} in some cells (~20%) but not in others (Fig. 4, *A* and *C*). In a few cases (~5% of cells), administration of ATP (1 μM) partially reverted the CCCP-induced oscillation stop (Fig. 4*C*). However, addition of ATP to the recording solution in the absence of serum was equally able to evoke Ca^{2+} oscillations in some cells (data not shown). The reason for this

effect is currently unknown; ATP might act on receptors on the surface of prMC but was also shown to cross the plasma membrane and to have an impact from the intracellular side (58). Application of CCCP before serum administration led to an immediate fall in the basal c_{mito}, reaching a new plateau 1–2 min later; the fall in c_{mito} was accompanied by a visible small rise in c_{cyt} in ~20% of cells, indicative of a release of mitochondrial Ca^{2+} to the cytosolic compartment. In addition, CCCP also decreased the basal level in c_{cyt} (both at 100 and 10 μM), signifying that also the plasma membrane potential was affected. Serum readministration following CCCP (100 μM) treatment was still able to briefly elevate both c_{cyt} and c_{mito}, but the increase in c_{mito} was smaller compared with cells not treated with CCCP; moreover, c_{mito} returned quickly to the level reached after CCCP addition, *i.e.* not to basal levels before treatment (Fig. 4*D*). Serum readministration after treatment with the lower CCCP concentration (10 μM) evoked low amplitude Ca^{2+} oscillations, and the mitochondrial Ca^{2+} rise during a cytosolic Ca^{2+} spike was small, and c_{mito} immediately returned to levels before serum administration but to lower levels than the basal c_{mito} before CCCP administration (Fig. 4*E*). The model also correctly predicted that the collapse in $\Delta\Psi$ (at $t = 3$ min) resulted in a lower c_{mito}. Serum administration (modeled as increasing J_{IN} and c_{IP3}) led to an increase in c_{cyt} and c_{mito} followed by oscillations in c_{cyt} and c_{mito} (Fig. 4, compare *F* with the experimental recording shown in *E*). To provide more evidence for the presence of $\Delta\Psi$-independent mitochondrial Ca^{2+} uptake as shown in Fig. 4*D*, we induced Ca^{2+} release from the ER by thapsigargin after CCCP administration (Fig. 4*G*). We observed a rise not only as expected in c_{cyt} but in parallel also in c_{mito}, confirming the existence of a $\Delta\Psi$-independent mitochondrial Ca^{2+} uptake. Addition of 1% FCS also resulted in an increase in the intracellular ATP concentration that lasted during the entire period of Ca^{2+} oscillations. Shortly after the collapse of $\Delta\Psi$ induced by CCCP, an immediate fall in ATP levels was observed (Fig. 4*H*). Overall, our findings indicate that the oscillation stop induced by the protonophore CCCP is not exclusively the result of the decreased mitochondrial Ca^{2+} uptake but also mediated via CCCP-induced changes in plasmalemmal Ca^{2+} influx and decreased ATP production.

The Role of Ca^{2+} Influx on Ca^{2+} Oscillations and on Mitochondrial Ca^{2+} Handling—A decrease in extracellular $[Ca^{2+}]$ by the addition of 0.25 mM EGTA to the extracellular solution resulted in a reduction in the oscillation frequency (Fig. 5*A*). In this condition, *i.e.* when c_{cyt} oscillations were not blocked completely, the amplitude of the Ca^{2+} signals was not affected, and the pattern of mitochondrial Ca^{2+} release/uptake was not affected (Fig. 5*A*). This could be accurately modeled in our simulation (Fig. 5*B*). When oscillations were induced by the addition of 1% FCS to the Ca^{2+}-containing recording solutions ($[Ca^{2+}]_o \approx 1$ mM), decreasing $[Ca^{2+}]_o$ to <1 μM by the addition of 10 mM EGTA at $t = 9$ min resulted in an immediate stop of the oscillations, indicating the necessity of Ca^{2+} influx for the oscillations in c_{cyt} (Fig. 5*C*). Removal of the extracellular Ca^{2+} had no visible effect on the decay curve of c_{mito}, and basal levels were reached at the end of the observation period (15 min). When the serum readministration was carried out in the "Ca^{2+}-free" condition, most prMC did not show any response in c_{cyt}. In ~5% of prMC, an initial small rise in c_{cyt} was observed but without signs of Ca^{2+} oscillations in support of the hypothesis that extracellular Ca^{2+} is essential for the sustained oscillations (Fig. 5*E*). Interestingly, different results were obtained in the Ca^{2+}-free condition when both Ca^{2+} influx and efflux across the plasma membrane were blocked by the addition of 1 mM La^{3+}, the so-called lanthanum insulation (19, 59), prior to the serum readministration. After serum addition, an immediate rise in c_{cyt} and c_{mito} was detected; although c_{cyt} decayed to basal levels within the next 2 min, c_{mito} remained elevated and did not show the typical decay curve as seen *e.g.* in Fig. 5*A*, *C*, and *E*. Moreover, long lasting but slow oscillations in c_{cyt} were observable (Fig. 5*G*), and at each cytosolic Ca^{2+} spike, a corresponding spike in c_{mito} occurred. This indicates that during the La^{3+} insulation a considerable amount of Ca^{2+} ions released from the ER, leading to the transient increase in c_{cyt}, is taken up by mitochondria as evidenced by the mitochondrial Ca^{2+} spikes (Fig. 5*G*). Thus, blocking the Ca^{2+} efflux across the plasma membrane leads to a shuttling of the Ca^{2+} ions between the ER and mitochondria, leading to these slow oscillations. Of note, the mitochondria remain in a rather Ca^{2+}-loaded state because Ca^{2+} cannot be transported out of the cell. We estimate that the mitochondrial Ca^{2+} uptake and release velocities likely determine the frequency of Ca^{2+} oscillations. La^{3+}-induced blocking of the Ca^{2+} transport across the plasma membrane at a time point when serum-induced Ca^{2+} oscillations were ongoing led to a complete block of the oscillations (Fig. 5, *I* and *K*). In some cases, La^{3+} treatment caused a final longer lasting Ca^{2+} spike (Fig. 5*K*), whereas in other prMC, La^{3+} completely blocked any further spikes (Fig. 5*I*). In all cases, the mathematical model could truthfully recapitulate the experimental findings by changing the parameters J_{IN} and J_{EFF} at different time points (Fig. 5, *D*, *F*, *H*, *J*, and *L*). Of note during La^{3+} insulations, the width (duration) of Ca^{2+} spikes was wider (longer) both *in vitro* and *in silico*. Moreover, the La^{3+}-evoked oscillation block in the presence of extracellular Ca^{2+} ($[Ca^{2+}]_o \approx 1$ mM) is, according to our model, mostly due to the decreased levels of Ca^{2+} ions present in the different cell compartments; *i.e.* the sum of $c_{cyt} + c_{ER} + c_{mito}$ is smaller than the sum prior to agonist administration.

Effect of the Intracellular Buffer Calretinin on Ca^{2+} Oscillations—Based on previous findings that human mesothelioma *in vivo*, mesothelioma cells *in vitro*, and reactive mesothelial cells express calretinin (60, 61), we hypothesized that prMC also might express this protein and that its presence might affect the Ca^{2+} oscillations. However, calretinin protein expression levels in prMC were found to be below the detection limit of our Western blot analysis (8), *i.e.* lower than ~100 nM and thus unlikely to affect the Ca^{2+} oscillations as the result of the Ca^{2+}-buffering capacity of calretinin. In support of this assumption, oscillation patterns (frequency, amplitude, and duration) in prMC from either wild type or calretinin knockout (CR−/−) mice were indistinguishable (data not shown). However, to mimic the situation of calretinin-expressing reactive mesothelial cells and to investigate the putative role of calretinin in those cells, we overexpressed a fusion protein consisting of EBFP separated from full-length calretinin by a small linker peptide by infection of prMC with the appropriate lenti-

virus. We estimated in a semiquantitative way by Western blot analyses the expression levels of EBFP-calretinin. The expression level was found to be ~75 pg of EBFP-calretinin/μg of total protein, leading to an estimated upper concentration of 250 μM calretinin. The EBFP tag on calretinin served as a marker for the distinction of the two populations with or without calretinin

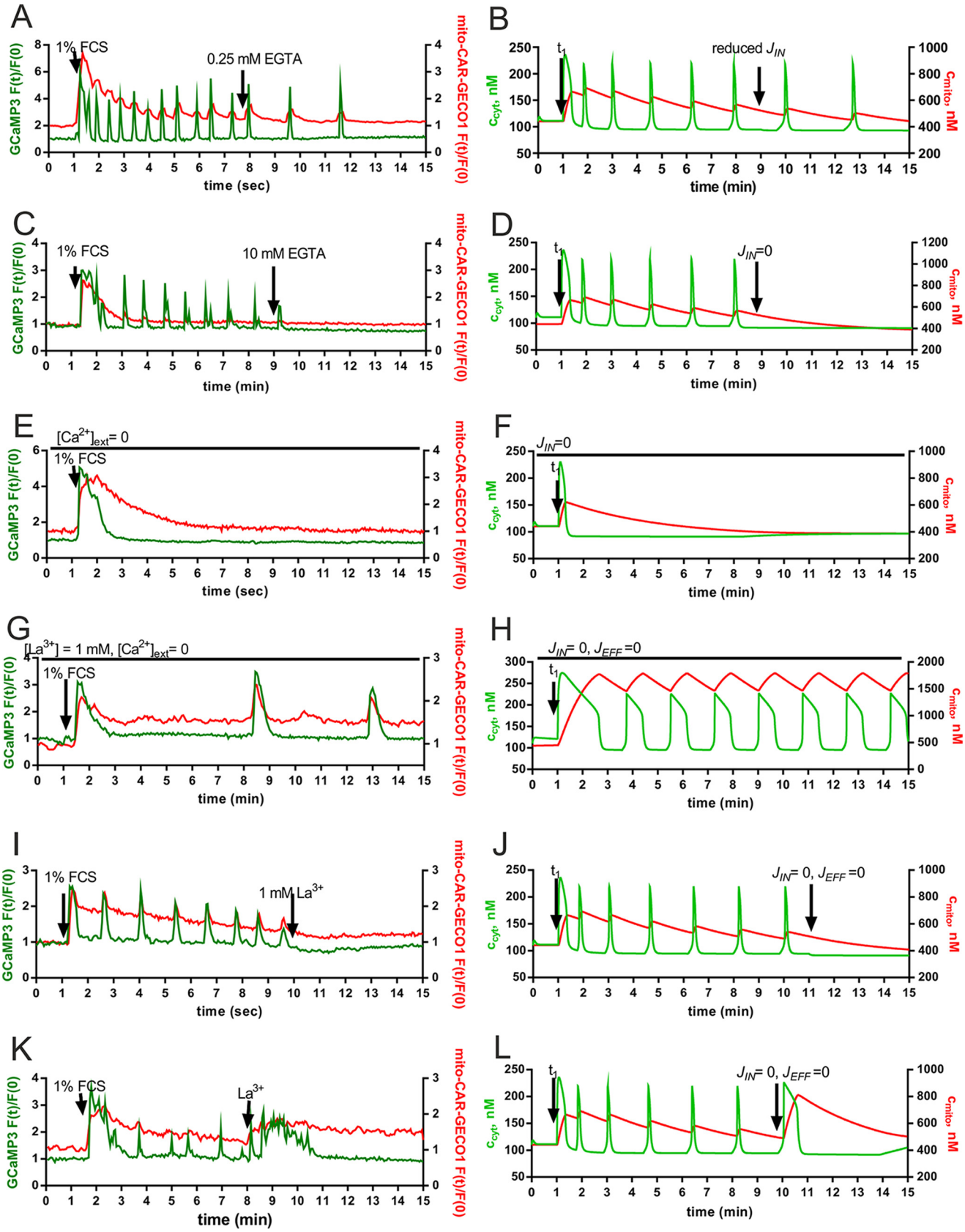

(Fig. 6*A*). The percentage of infected cells was usually higher than 90%. The fraction of prMC showing Ca^{2+} oscillations (~10–20%) was considerably lower than in non-infected cells not expressing calretinin (~60–70%) and moreover was restricted to cells showing faint blue fluorescence, *i.e.* low EBFP-calretinin expression levels. In the oscillating EBFP-calretinin-expressing prMC, the Ca^{2+} spike amplitudes were smaller, and the half-width of Ca^{2+} spikes (duration) was increased (Fig. 6*B*). The largest effect caused by EBFP-calretinin was the reduction of the amplitude of the first Ca^{2+} spike after serum readministration (Fig. 6*C*); on average it was half the size compared with the situation without calretinin. Likely as the consequence of the reduction in c_{cyt}, the increase in c_{mito} also was clearly diminished (Fig. 6*D*). The frequency of oscillation slightly decreased (~10–20% reduction in each time segment). Our model simulations incorporating calretinin with the known Ca^{2+} binding characteristics (54) showed similar modifications: a decrease both in the amplitudes of c_{cyt} spikes and in the amount of mitochondrial Ca^{2+} uptake (Fig. 6*E*). In our model, an increase in calretinin concentration resulted in an increase of the oscillation frequency, a prediction not supported by our experimental findings. One reason may be that calretinin, in addition to its buffering capacity, might act as a Ca^{2+} sensor in prMC. We had previously shown that calretinin is able to directly modify the activity of a Ca^{2+} channel (60), and direct targets for calretinin implicated in Ca^{2+} transportation might also be present in prMC. As a control to exclude that observed effects were mediated by the EBFP part of the fusion protein, prMC were infected with the lentivirus LV-EBFP2-X leading to the expression of EBFP only. No differences in the Ca^{2+} oscillations patterns were observed between cells expressing EBFP and non-infected control cells (data not shown). Based on the fact that Ca^{2+} oscillations in EBFP-calretinin-expressing cells were limited to those with faint fluorescence, we reasoned that the concentration in these cells was ~10-fold (*e.g.* 25 μM) lower than the global concentration (250 μM) estimated from Western blot analyses. Thus, we tested whether the commonly used synthetic Ca^{2+} chelators BAPTA and EGTA, which have different properties (*e.g.* K_d, on-rate constant (k_{on}), and diffusion coefficient (D)) than calretinin, were able to recapitulate the effects of calretinin. In prMC loaded with BAPTA-AM (30 μM), serum readministration evoked a slow and prolonged c_{cyt} elevation paralleled by a minute increase in c_{mito} (Fig. 6*F*). Most importantly, the initial rise in c_{cyt} as also seen in EBFP-calretinin-expressing prMC (Fig. 6*C*) was completely abolished. In contrast, after EGTA-AM loading serum, readministration induced a short spike both in c_{cyt} and c_{mito} (Fig. 6*E*) followed by a rapid return to essentially baseline levels. No Ca^{2+} oscillations were observed in both cases. This further indicates that the properties of calretinin are clearly distinct from those of either BAPTA or EGTA.

Discussion

Characteristics of mitochondrial Ca^{2+} transport have not been examined in detail in most cell types. The main reason why we know relatively little about mitochondrial Ca^{2+} handling is because the molecular identity of the channels involved in mitochondrial transport have only recently been discovered (18, 62, 63), and specifically targeted, pH- and $\Delta\Psi$-insensitive Ca^{2+} indicators are only currently available (23). Nevertheless, there are few models for Ca^{2+} oscillations where the function of mitochondrial Ca^{2+} uptake has been taken into account (64).

Our experiments affirm previous data that mitochondria, even at the resting state, are able to transport and store Ca^{2+} ions (65). The fast release of the stored Ca^{2+} from the mitochondria due to the decrease/collapse of the membrane potential indicates that the strongly negative $\Delta\Psi$ ensures a constant Ca^{2+} uptake into the mitochondria. This uptake is in a steady-state equilibrium with the constant Ca^{2+} efflux mediated by the mitochondrial exchangers (66), and the efflux is an electrogenic process (67). The electrochemical proton gradient across the inner mitochondrial is used to remove the excess Ca^{2+} ions (68). Our recordings show that this basal steady-state mitochondrial Ca^{2+} concentration can fluctuate, showing "spontaneous" mitochondrial Ca^{2+} spikes. Most probably this is mediated by an endogenous MCU activator that has not been identified at the molecular level yet. Ca^{2+} transients in c_{cyt} were previously reported to evoke an increase in c_{mito}, activating both cytoplasmic (19) and mitochondrial enzymes (2). Thus, Ca^{2+} transients observed selectively in c_{mito} in some prMC (Fig. 2*A*) might allow for the autonomous activation of mitochondrial enzymes. The Ca^{2+} ions causing the mitochondrial spike are likely to originate from the cytosolic compartment; however, our results indicate that the amount of Ca^{2+} ions responsible for the increase in c_{mito} was not sufficient to be detected as a decrease in c_{cyt}. Alternatively, at basal conditions, the equilibrium level of c_{cyt} might be regulated by a rather rapid constant exchange of Ca^{2+} ions among the cytosol, the extracellular space, and/or the ER compartment.

The Ca^{2+} oscillation models usually differ in how they simulate the functions of $InsP_3R$, the channel that transports Ca^{2+} ions from the ER to the cytosol. The "c_{cyt}/[$InsP_3$]" models (for a review, see Ref. 69) postulate that the $InsP_3R$ has a binding site

FIGURE 5. **Modulation of Ca^{2+} transport across the plasma membrane: representative experimental findings (*left panels*) and model simulations (*right panels*).** *A*, a decrease in external [Ca^{2+}] from 1 to ~0.75 mM by administration of 0.25 mM EGTA results in a decreased oscillation frequency. *B*, the model was able to recapitulate the effect of reduction of Ca^{2+} influx on Ca^{2+} oscillations. The parameter $r_{IN,p}$ representing J_{IN} was reduced from 0.85 to 0.6 nM/s at $t = 9$ min. *C*, removal of extracellular Ca^{2+} by the addition of EGTA (10 mM) at $t = 9$ min resulted in one final Ca^{2+} spike before cessation of oscillations. *D*, the model correctly predicted an immediate stop in Ca^{2+} oscillations when J_{IN} was decreased to zero. *E*, in the absence of extracellular Ca^{2+} ($[Ca^{2+}]_o < 1$ μM), prMC did not show Ca^{2+} oscillations. In a few cells, a single Ca^{2+} transient was visible. *F*, model traces for c_{cyt} (*green*) and c_{mito} (*red*) in "zero Ca^{2+}" ($J_{IN} = 0$) confirmed the experimental findings shown in *E*. *G*, addition of Lanthanum chloride (La^{3+} insulation) prior to serum administration rendered Ca^{2+} oscillations independent of extracellular Ca^{2+} ions. Note that (i) c_{mito} remained elevated during the entire period (no slow decay phase), (ii) the frequency of Ca^{2+} oscillations was lower than in control conditions (*e.g.* as shown in the initial period in *A* or *C*), and (iii) the half-width of Ca^{2+} transients representing the duration of a Ca^{2+} spike was increased. *H*, the model confirmed that mitochondria were able to substitute for the role of the extracellular Ca^{2+} reservoir during Ca^{2+} oscillations. In line with the experimental findings, the half-width of Ca^{2+} spikes was increased, and c_{mito} remained elevated. *I–K*, La^{3+} insulation induced after serum administration (at $t \approx 8$–10 min) blocked the Ca^{2+} oscillations either with (*K*) or without (*I*) a final large Ca^{2+} transient. *J–L*, the model was able to recapitulate both phenomena: it revealed that c_{TOTAL}, *i.e.* the total amount of Ca^{2+} ions in the cell ($c_{mito} + c_{cyt} + c_{ER}$), determined the response to La^{3+} insulation.

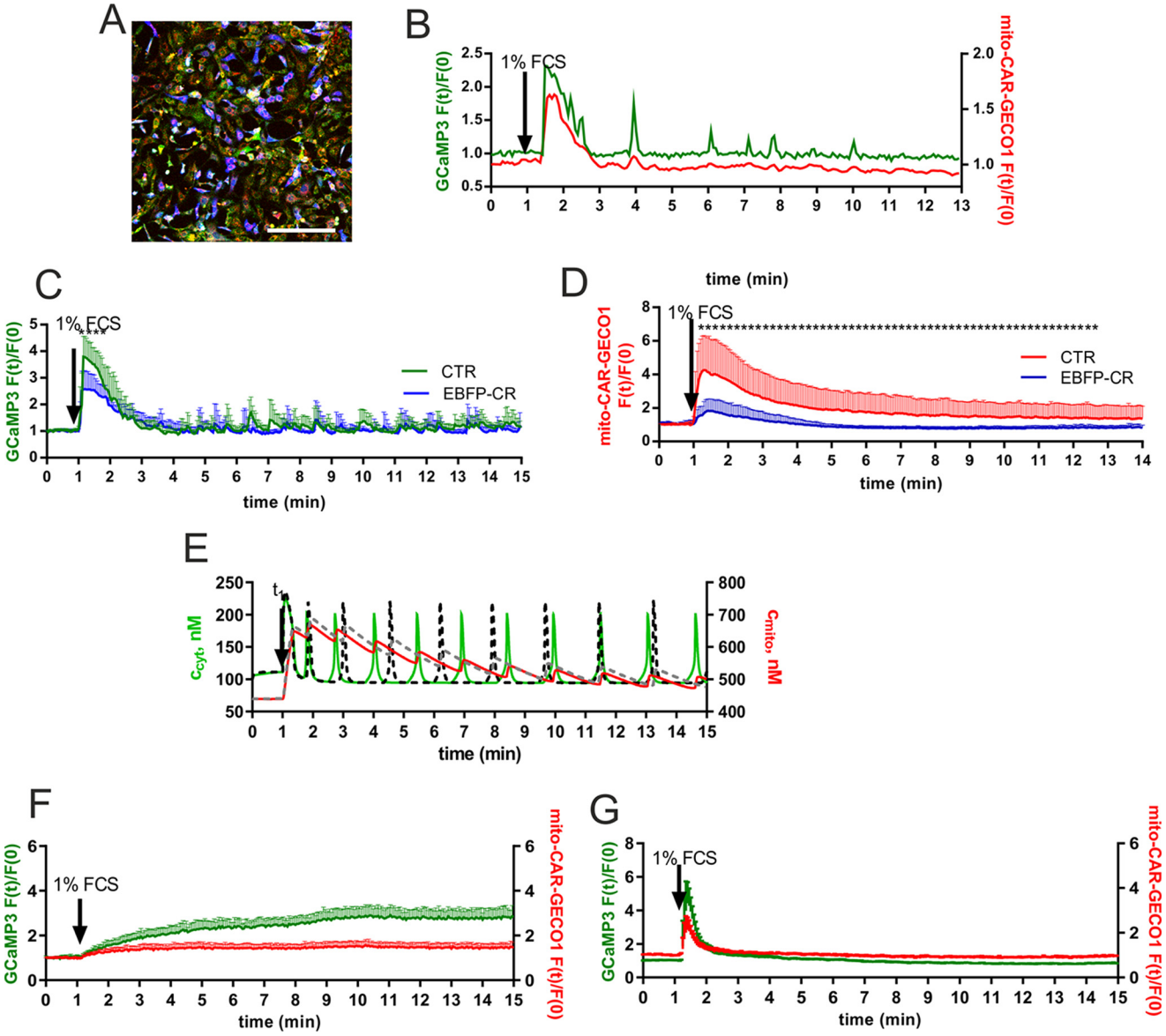

FIGURE 6. **The effect of increased mobile cytosolic Ca^{2+}-buffering capacity resulting from ectopic EBFP-calretinin expression on Ca^{2+} oscillations.** *A*, fluorescence image of cultured prMC expressing the fusion protein EFBP-calretinin (*blue*). The faint *green* and *red* fluorescence signals represent the basal fluorescence intensities of GCaMP3 (cytosolic Ca^{2+} indicator) and mito-CAR-GECO1 (mitochondrial Ca^{2+} indicator), respectively. The faintly fluorescent *non-blue* cells are control cells not expressing EFBP-calretinin. The *scale bar* represents 250 μm. *B*, single cell fluorescence intensity recordings from time lapse videos show a representative Ca^{2+} response in c_{cyt} and c_{mito} of cells expressing EBFP-calretinin. Oscillations were only observed in cells with faint *blue* fluorescence, *i.e.* relatively low EBFP-calretinin expression levels. Note the relatively small signal in c_{cyt} as compared with control cells (*e.g.* in Figs. 2*C* and 4*B*). *C*, Ca^{2+} oscillations were monitored in a mixed population of mito-CAR-GECO1/GCaMP3 prMC (*green* trace) and EBFP-calretinin/mito-CAR-GECO1/GCaMP3 prMC (*black* trace). Averages of c_{cyt} values of 10 randomly selected oscillatory prMC each were plotted; data are mean + S.D. Serum-induced maximal amplitudes in c_{cyt} were considerably lower in EBFP-calretinin-expressing prMC. *D*, a similar reduction was also seen for c_{mito} in oscillatory prMC; data are mean + S.D. from eight cells each. *E*, in the simulation, the known Ca^{2+} binding properties of calretinin were incorporated. The addition of calretinin (0.5 μM) resulted in lower amplitudes of c_{cyt}, and the mitochondrial uptake (reflected by c_{mito}) was decreased in the presence of calretinin. *F*, BAPTA-AM preloading (30 μM for 15 min) resulted in a low amplitude plateau response in c_{cyt} (*green*) and an even smaller one in c_{mito} without Ca^{2+} oscillations. Also the initial serum-induced Ca^{2+} spike was completely abolished. *G*, in EGTA-AM preloaded (30 μM for 15 min) prMC, serum readministration evoked single Ca^{2+} spikes of short duration in c_{cyt} (*green*) and c_{mito} (*red*). Only a few cells (<1%) showed a second Ca^{2+} transient, but oscillations in c_{cyt} were completely blocked by 30 μM EGTA. *F* and *G*, averages of c_{cyt} and c_{mito} values of 10 randomly selected prMC were plotted; data are mean + S.D. *Asterisks* indicate significance at $p < 0.05$. *Error bars* represent S.D. *CTR*, control.

for $InsP_3$, an activating binding site for Ca^{2+}, and an inhibiting binding site for Ca^{2+}. In these models, all binding sites are localized on the cytoplasmic side, and the function of $InsP_3$ does not depend on c_{ER}. Binding of Ca^{2+} to the activating site and of $InsP_3$ to the $InsP_3$ binding site opens the channel, whereas Ca^{2+} binding to the inhibiting site closes the InP_3R. Moreover, the binding of Ca^{2+} to the inhibiting site occurs rather slowly and with a lower affinity as compared with the activating site, subsequently resulting in oscillations in c_{cyt}. In these models, the $InsP_3$ concentration uniquely determines the oscillation frequency (70). In the "store loading" models (also called "c_{cyt}/c_{ER}" models), the function of $InsP_3R$ depends not only on c_{cyt} but also on c_{ER}. In these models, the Ca^{2+} influx across the plasma membrane plays a critical role in determining

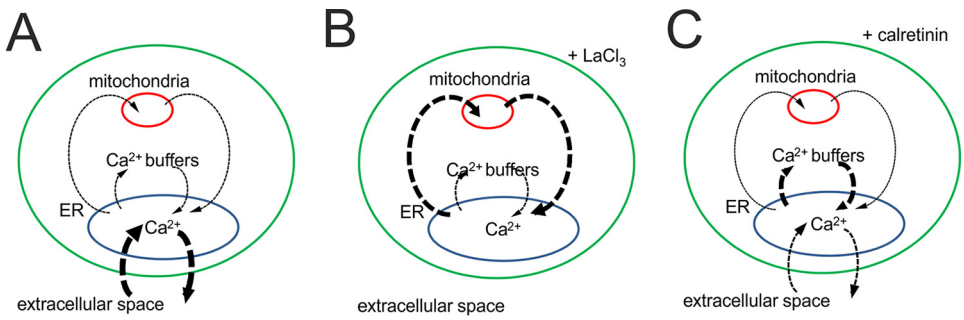

FIGURE 7. **Contribution of Ca^{2+} signaling toolkit components to serum-induced Ca^{2+} oscillations in prMC.** *A*, in unperturbed (control) prMC *in vitro*, Ca^{2+} oscillations are primarily the result of the interplay between Ca^{2+} from the extracellular space and the ER with some minor contributions of mitochondria. The *arrows* indicate the shuttling of Ca^{2+} ions between the different compartments (the *thicker* the *arrow*, the more important is this pathway). In prMC, expression of calretinin is virtually absent, excluding an important role of this protein with respect to mobile Ca^{2+} buffering. *B*, if cells are subjected to La^{3+} insulation excluding the exchange of Ca^{2+} ions via the plasma membrane, the repetitive Ca^{2+} exchange between the ER and mitochondria allows for the generation of Ca^{2+} oscillations. *C*, the addition of the mobile Ca^{2+} buffer calretinin as observed in reactive mesothelial cells and mesothelioma cells affects Ca^{2+} oscillations. High expression levels (>1 μM in our model) completely block oscillations; lower levels (≈0.5 μM) reduce the amplitude of c_{cyt} as well as of c_{mito} during Ca^{2+} oscillations; *i.e.* calretinin competes with mitochondria, thus reducing the shuttling of Ca^{2+} ions between the ER and mitochondria.

the oscillation frequency (8, 71, 72). At a constant [$InsP_3$], the duration of the interspike period is determined by the velocity of cellular Ca^{2+} replenishment, which is manifested as a continuous ER loading together with a constant basal c_{cyt}. The experimentally observable sawtooth wave oscillations in c_{ER} during the cytoplasmic baseline spiking oscillations are an important argument in favor of the store loading theory (8). However, the store loading-based models cannot cope with the fact that in some cells the Ca^{2+} oscillations do not depend on Ca^{2+} influx across the plasma membrane. Our experiments and modeling studies revealed that the incorporation of mitochondria as an additional Ca^{2+} source/store in the store loading-based models considerably augments the quality of the simulations. That is, the modeling predictions are more congruent with the experimental findings, which allows for a better mechanistic understanding. The mitochondrial Ca^{2+} transport enables the store loading-based models also to display Ca^{2+} oscillation in the absence of extracellular Ca^{2+}.

The simulation of the La^{3+} insulation was previously endeavored by Sneyd *et al.* (73). Although their model does not contain mitochondria and moreover c_{cyt} is continuously decreasing during the oscillations, their model reveals important aspects of the Ca^{2+} oscillations, namely their dependence on the total Ca^{2+} load of the cell. In their model, the cell has a high resting Ca^{2+}; upon agonist stimulation, the activation of plasma membrane Ca^{2+}-ATPases causes a net loss of Ca^{2+} from the cells even though the Ca^{2+} influx is augmented after stimulation (73). A similar phenomenon is also observed in our model; the total cellular Ca^{2+} content ($c_{cyt} + c_{ER} + c_{mito}$) determines the response to the La^{3+} insulation; blocking of the Ca^{2+} influx and efflux results in an oscillation stop that can either occur after a final Ca^{2+} spike or directly after La^{3+} addition, *i.e.* without a change in c_{cyt}. In contrast to the previous model (73), basal c_{cyt} levels during the interspike phase of the oscillations remain constant. This is in line with the experiments carried out by us and others (74).

Shuttling of Ca^{2+} ions between the ER and mitochondria was experimentally demonstrated in the study of Ishii *et al.* (9). They reported that in HeLa cells the cycles of ER/mitochondrion shuttling are repeated until c_{mito} has reached the basal level prior to the stimulation. In our study with prMC, we observed Ca^{2+} oscillation even (i) when c_{mito} had reached its basal levels or (ii) if c_{mito} had been considerably lowered by CCCP administration. One has to keep in mind that CCCP also results in the collapse of the plasma membrane potential (75), which subsequently reduces the plasmalemmal Ca^{2+} influx (76). Thus, one reason for the CCCP-evoked stop in oscillations might be a disturbed Ca^{2+} influx. Moreover, the CCCP-mediated drop in ATP production likely leading to an impairment of the ER Ca^{2+} transport might also contribute to the oscillation arrest (77); *i.e.* the effects of protonophores are not exclusively attributed to the reduced mitochondrial Ca^{2+} uptake as was proposed in earlier studies (9). When CCCP was administered before serum, it caused a Ca^{2+} transient due to the mitochondrial release, which was followed by a period of lower resting c_{cyt}. A lower c_{cyt} is a sign of the reduced Ca^{2+} influx (resting plasmalemmal Ca^{2+} leakage). There was a similar decrease in resting c_{cyt} when the extracellular free Ca^{2+} was chelated by EGTA (data not shown).

The Ca^{2+} influx across the plasma membrane is important to sustain the Ca^{2+} oscillations in prMC (78) but not in HeLa cells (9). The different dependence of these cell types on extracellular Ca^{2+} for the oscillations might be the result of differences in the contribution/importance of the various Ca^{2+} shuttling pathways between ER and mitochondria on the one hand and between ER and the extracellular space on the other. Our results indicate that plasmalemmal Ca^{2+} extrusion systems and mitochondrial Ca^{2+} uptake channels compete for the Ca^{2+} ions released from the ER. We hypothesize that in some cells, such as prMC and HEK cells (74), the shuttling between the extracellular space and the ER dominates over the shuttling between mitochondria and the ER. However, in HeLa cells and hepatocytes, the ER/mitochondrion shuttling prevails. This might explain why Ca^{2+} oscillations in some cells are strongly dependent on extracellular Ca^{2+} ions but not in others.

Another often neglected aspect about "Ca^{2+} shuttling" pathways is the contribution of cytosolic Ca^{2+} buffers present at rather high concentrations in the cytosol of some cell types. They are expected to modulate the Ca^{2+} shuttling among all compartments, extracellular space, ER, and mitochondria, as well as to transiently affect c_{cyt} (Fig. 7). A strong interdependence between cytoplasmic Ca^{2+} buffers and mitochondria has

been demonstrated before. The expression levels of parvalbumin, a Ca^{2+}-buffering protein with slow binding kinetics, and the mitochondrial volume in fast twitch muscle cells and in parvalbumin-expressing neurons are inversely regulated (Ref. 79, and for more details, see Ref. 80). In our study, we observed that overexpression of calretinin modifies Ca^{2+} signals and associated oscillations. It reduces the amount of Ca^{2+} ions shuttling both between the ER and mitochondria and between the ER and the cytoplasm. Our model predicts that at calretinin concentrations >1 μM Ca^{2+} oscillations should be blocked in prMC. This is in apparent contradiction with the experimental results where oscillations still existed in EBFP-calretinin-expressing cells likely expressing levels higher than 1 μM (Fig. 6). However, in our modeling, the Ca^{2+} microdomain was not considered, and Ca^{2+} binding characteristics of calretinin (*e.g.* K_d and k_{on}) might be different in the cytosol of prMC than the parameters determined *in vitro* (34). Furthermore, adaptation/compensation mechanisms might be induced in prMC overexpressing calretinin that would still allow for the generation of Ca^{2+} oscillations.

Of relevance, calretinin reduced the mitochondrial Ca^{2+} uptake and Ca^{2+} accumulation. In human malignant mesothelioma, mostly of the epithelioid type, calretinin is overexpressed (81). This might cause changes, *e.g.* a delay or blocking of apoptotic/necrotic processes (78, 82). Thus, the increased calretinin expression in mesothelioma cells and moreover in certain colon cancer (83) and derived cell lines (84) might be correlated or causally linked to the increased resistance of these tumor cells to the apoptotic/necrotic signals either occurring in healthy physiological conditions or resulting from treatment with chemotherapy drugs such as oxaliplatin or 5-fluorouracil (85). In support, colon cancer cells resistant to aurora kinase inhibitors are characterized by higher calretinin expression levels (86). Moreover, down-regulation of calretinin by lentiviral infection induces apoptosis in mesothelioma cell lines *in vitro* via an intrinsic mitochondrion-mediated pathway (87). Also down-regulation of calretinin in colon cancer cells is associated with cell growth arrest and increased apoptosis (88).

Author Contributions—L. P. designed the study, performed the experiments with simulations, and wrote the paper. W. B. provided assistance, contributed to lentivirus production and cloning (CALB2), and performed qRT-PCR. B. S. secured funding, analyzed data, and wrote the paper.

Acknowledgments—We are grateful to Simone Eichenberger and Valérie Salicio for excellent technical assistance as well as to Michael Dougoud, Department of Mathematics, University of Fribourg, for verifying the mathematical equations. We thank Dr. D. Trono (École Polytechnique Fédérale de Lausanne, Lausanne, Switzerland) for providing pLVTHM (Addgene plasmid 12247), pMD2G-VSVG (Addgene plasmid 12259), and psPAX2 (Addgene plasmid 12260); Dr. L. Looger for GCaMP3 (Addgene plasmid 22692); and Dr. R. E. Campbell for mito-CAR-GECO1 (Addgene plasmid 46022). pLV-EBF2-nuc was a gift from Dr. P. Tsoulfas (Addgene plasmid 36085).

References

1. Berridge, M. J., Bootman, M. D., and Roderick, H. L. (2003) Calcium signalling: dynamics, homeostasis and remodelling. *Nat. Rev. Mol. Cell Biol.* **4,** 517–529
2. Ivannikov, M. V., and Macleod, G. T. (2013) Mitochondrial free Ca^{2+} levels and their effects on energy metabolism in *Drosophila* motor nerve terminals. *Biophys. J.* **104,** 2353–2361
3. Rooney, T. A., Sass, E. J., and Thomas, A. P. (1989) Characterization of cytosolic calcium oscillations induced by phenylephrine and vasopressin in single fura-2-loaded hepatocytes. *J. Biol. Chem.* **264,** 17131–17141
4. Clapham, D. E., Lechleiter, J. D., and Girard, S. (1993) Intracellular waves observed by confocal microscopy from *Xenopus* oocytes. *Adv. Second Messenger Phosphoprotein Res.* **28,** 161–165
5. Yule, D. I., and Gallacher, D. V. (1988) Oscillations of cytosolic calcium in single pancreatic acinar cells stimulated by acetylcholine. *FEBS Lett.* **239,** 358–362
6. Martin, S. C., and Shuttleworth, T. J. (1994) Ca^{2+} influx drives agonist-activated $[Ca^{2+}]_i$ oscillations in an exocrine cell. *FEBS Lett.* **352,** 32–36
7. Estrada, M., Uhlen, P., and Ehrlich, B. E. (2006) Ca^{2+} oscillations induced by testosterone enhance neurite outgrowth. *J. Cell Sci.* **119,** 733–743
8. Pecze, L., and Schwaller, B. (2015) Characterization and modeling of Ca^{2+} oscillations in mouse primary mesothelial cells. *Biochim. Biophys. Acta* **1853,** 632–645
9. Ishii, K., Hirose, K., and Iino, M. (2006) Ca^{2+} shuttling between endoplasmic reticulum and mitochondria underlying Ca^{2+} oscillations. *EMBO Rep.* **7,** 390–396
10. Wu, Y. W., Tang, X., Arizono, M., Bannai, H., Shih, P. Y., Dembitskaya, Y., Kazantsev, V., Tanaka, M., Itohara, S., Mikoshiba, K., and Semyanov, A. (2014) Spatiotemporal calcium dynamics in single astrocytes and its modulation by neuronal activity. *Cell Calcium* **55,** 119–129
11. Lechleiter, J., Girard, S., Peralta, E., and Clapham, D. (1991) Spiral calcium wave propagation and annihilation in *Xenopus laevis* oocytes. *Science* **252,** 123–126
12. Frame, M. K., and de Feijter, A. W. (1997) Propagation of mechanically induced intercellular calcium waves via gap junctions and ATP receptors in rat liver epithelial cells. *Exp. Cell Res.* **230,** 197–207
13. Foreman, M. A., Smith, J., and Publicover, S. J. (2006) Characterisation of serum-induced intracellular Ca^{2+} oscillations in primary bone marrow stromal cells. *J. Cell. Physiol.* **206,** 664–671
14. Wood, A., Wing, M. G., Benham, C. D., and Compston, D. A. (1993) Specific induction of intracellular calcium oscillations by complement membrane attack on oligodendroglia. *J. Neurosci.* **13,** 3319–3332
15. Goustin, A. S., Leof, E. B., Shipley, G. D., and Moses, H. L. (1986) Growth factors and cancer. *Cancer Res.* **46,** 1015–1029
16. Sée, V., Rajala, N. K., Spiller, D. G., and White, M. R. (2004) Calcium-dependent regulation of the cell cycle via a novel MAPK-NF-κB pathway in Swiss 3T3 cells. *J. Cell Biol.* **166,** 661–672
17. Rizzuto, R., and Pozzan, T. (2006) Microdomains of intracellular Ca^{2+}: molecular determinants and functional consequences. *Physiol. Rev.* **86,** 369–408
18. De Stefani, D., Raffaello, A., Teardo, E., Szabò, I., and Rizzuto, R. (2011) A forty-kilodalton protein of the inner membrane is the mitochondrial calcium uniporter. *Nature* **476,** 336–340
19. Van Breemen, C., Farinas, B. R., Gerba, P., and McNaughton, E. D. (1972) Excitation-contraction coupling in rabbit aorta studied by the lanthanum method for measuring cellular calcium influx. *Circ. Res.* **30,** 44–54
20. Bot, J., Whitaker, D., Vivian, J., Lake, R., Yao, V., and McCauley, R. (2003) Culturing mouse peritoneal mesothelial cells. *Pathol. Res. Pract.* **199,** 341–344
21. Connell, N. D., and Rheinwald, J. G. (1983) Regulation of the cytoskeleton in mesothelial cells: reversible loss of keratin and increase in vimentin during rapid growth in culture. *Cell* **34,** 245–253
22. Tian, L., Hires, S. A., Mao, T., Huber, D., Chiappe, M. E., Chalasani, S. H., Petreanu, L., Akerboom, J., McKinney, S. A., Schreiter, E. R., Bargmann, C. I., Jayaraman, V., Svoboda, K., and Looger, L. L. (2009) Imaging neural activity in worms, flies and mice with improved GCaMP calcium indicators. *Nat. Methods* **6,** 875–881
23. Wu, J., Liu, L., Matsuda, T., Zhao, Y., Rebane, A., Drobizhev, M., Chang, Y. F., Araki, S., Arai, Y., March, K., Hughes, T. E., Sagou, K., Miyata, T., Nagai, T., Li, W. H., and Campbell, R. E. (2013) Improved orange and red Ca^{2+} indicators and photophysical considerations for optogenetic appli-

cations. *ACS Chem. Neurosci.* **4,** 963–972
24. Wiznerowicz, M., and Trono, D. (2003) Conditional suppression of cellular genes: lentivirus vector-mediated drug-inducible RNA interference. *J. Virol.* **77,** 8957–8961
25. D'Orlando, C., Fellay, B., Schwaller, B., Salicio, V., Bloc, A., Gotzos, V., and Celio, M. R. (2001) Calretinin and calbindin D-28k delay the onset of cell death after excitotoxic stimulation in transfected P19 cells. *Brain Res.* **909,** 145–158
26. Kutner, R. H., Zhang, X. Y., and Reiser, J. (2009) Production, concentration and titration of pseudotyped HIV-1-based lentiviral vectors. *Nat. Protoc.* **4,** 495–505
27. Blum, W., Pecze, L., Felley-Bosco, E., Worthmüller-Rodriguez, J., Wu, L., Vrugt, B., de Perrot M., Schwaller B. (2015) Establishment of immortalized murine mesothelial cells and a novel mesothelioma cell line. *In Vitro Cell. Dev. Biol. Anim.* **51,** 714–721
28. Milo, R. (2013) What is the total number of protein molecules per cell volume? A call to rethink some published values. *BioEssays* **35,** 1050–1055
29. Manford, A. G., Stefan, C. J., Yuan, H. L., Macgurn, J. A., and Emr, S. D. (2012) ER-to-plasma membrane tethering proteins regulate cell signaling and ER morphology. *Dev. Cell* **23,** 1129–1140
30. Rizzuto, R., Pinton, P., Carrington, W., Fay, F. S., Fogarty, K. E., Lifshitz, L. M., Tuft, R. A., and Pozzan, T. (1998) Close contacts with the endoplasmic reticulum as determinants of mitochondrial Ca^{2+} responses. *Science* **280,** 1763–1766
31. Dupont, G., Abou-Lovergne, A., and Combettes, L. (2008) Stochastic aspects of oscillatory Ca^{2+} dynamics in hepatocytes. *Biophys. J.* **95,** 2193–2202
32. al-Baldawi, N. F., and Abercrombie, R. F. (1995) Calcium diffusion coefficient in *Myxicola* axoplasm. *Cell Calcium* **17,** 422–430
33. Young, R. C., and Zhang, P. (2001) The mechanism of propagation of intracellular calcium waves in cultured human uterine myocytes. *Am. J. Obstet. Gynecol.* **184,** 1228–1234
34. Fridlyand, L. E., Tamarina, N., and Philipson, L. H. (2003) Modeling of Ca^{2+} flux in pancreatic β-cells: role of the plasma membrane and intracellular stores. *Am. J. Physiol. Endocrinol. Metab.* **285,** E138–E154
35. Caride, A. J., Penheiter, A. R., Filoteo, A. G., Bajzer, Z., Enyedi, A., and Penniston, J. T. (2001) The plasma membrane calcium pump displays memory of past calcium spikes. Differences between isoforms 2b and 4b. *J. Biol. Chem.* **276,** 39797–39804
36. Fink, C. C., Slepchenko, B., Moraru, I. I., Watras, J., Schaff, J. C., and Loew, L. M. (2000) An image-based model of calcium waves in differentiated neuroblastoma cells. *Biophys. J.* **79,** 163–183
37. Herrington, J., Park, Y. B., Babcock, D. F., and Hille, B. (1996) Dominant role of mitochondria in clearance of large Ca^{2+} loads from rat adrenal chromaffin cells. *Neuron* **16,** 219–228
38. Chandrasekera, P. C., Kargacin, M. E., Deans, J. P., and Lytton, J. (2009) Determination of apparent calcium affinity for endogenously expressed human sarco(endo)plasmic reticulum calcium-ATPase isoform SERCA3. *Am. J. Physiol. Cell Physiol.* **296,** C1105–C1114
39. Turovsky, E. A., Kaimachnikov, N. P., Turovskaya, M. V., Berezhnov, A. V., Dynnik, V. V., and Zinchenko, V. P. (2012) Two mechanisms of calcium oscillations in adipocytes. *Biochemistry (Moscow)* **6,** 26–34
40. Sienaert, I., De Smedt, H., Parys, J. B., Missiaen, L., Vanlingen, S., Sipma, H., and Casteels, R. (1996) Characterization of a cytosolic and a luminal Ca^{2+} binding site in the type I inositol 1,4,5-trisphosphate receptor. *J. Biol. Chem.* **271,** 27005–27012
41. Horne, J. H., and Meyer, T. (1995) Luminal calcium regulates the inositol trisphosphate receptor of rat basophilic leukemia cells at a cytosolic site. *Biochemistry* **34,** 12738–12746
42. Sienaert, I., Missiaen, L., De Smedt, H., Parys, J. B., Sipma, H., and Casteels, R. (1997) Molecular and functional evidence for multiple Ca^{2+}-binding domains in the type 1 inositol 1,4,5-trisphosphate receptor. *J. Biol. Chem.* **272,** 25899–25906
43. Missiaen, L., De Smedt, H., Parys, J. B., and Casteels, R. (1994) Co-activation of inositol trisphosphate-induced Ca^{2+} release by cytosolic Ca^{2+} is loading-dependent. *J. Biol. Chem.* **269,** 7238–7242
44. Mak, D. O., McBride, S., and Foskett, J. K. (2001) Regulation by Ca^{2+} and inositol 1,4,5-trisphosphate (InsP3) of single recombinant type 3 InsP3 receptor channels. Ca^{2+} activation uniquely distinguishes types 1 and 3 insp3 receptors. *J. Gen. Physiol.* **117,** 435–446
45. Kaftan, E. J., Ehrlich, B. E., and Watras, J. (1997) Inositol 1,4,5-trisphosphate (InsP3) and calcium interact to increase the dynamic range of InsP3 receptor-dependent calcium signaling. *J. Gen. Physiol.* **110,** 529–538
46. Joseph, S. K., Rice, H. L., and Williamson, J. R. (1989) The effect of external calcium and pH on inositol trisphosphate-mediated calcium release from cerebellum microsomal fractions. *Biochem. J.* **258,** 261–265
47. Tanimura, A., and Turner, R. J. (1996) Inositol 1,4,5-trisphosphate-dependent oscillations of luminal [Ca^{2+}] in permeabilized HSY cells. *J. Biol. Chem.* **271,** 30904–30908
48. Zimmermann, B. (2000) Control of InsP3-induced Ca^{2+} oscillations in permeabilized blowfly salivary gland cells: contribution of mitochondria. *J. Physiol.* **525,** 707–719
49. Camello, C., Lomax, R., Petersen, O. H., and Tepikin, A. V. (2002) Calcium leak from intracellular stores—the enigma of calcium signalling. *Cell Calcium* **32,** 355–361
50. Marhl, M., Schuster, S., and Brumen, M. (1998) Mitochondria as an important factor in the maintenance of constant amplitudes of cytosolic calcium oscillations. *Biophys. Chem.* **2,** 125–132
51. Gunter, T. E., and Pfeiffer, D. R. (1990) Mechanisms by which mitochondria transport calcium. *Am. J. Physiol. Cell Physiol.* **258,** C755–C786
52. Shuttleworth, T. J., and Mignen, O. (2003) Calcium entry and the control of calcium oscillations. *Biochem. Soc. Trans.* **31,** 916–919
53. Tanimura, A., Morita, T., Nezu, A., Shitara, A., Hashimoto, N., and Tojyo, Y. (2009) Use of fluorescence resonance energy transfer-based biosensors for the quantitative analysis of inositol 1,4,5-trisphosphate dynamics in calcium oscillations. *J. Biol. Chem.* **284,** 8910–8917
54. Faas, G. C., Schwaller, B., Vergara, J. L., and Mody, I. (2007) Resolving the fast kinetics of cooperative binding: Ca^{2+} buffering by calretinin. *PLoS Biol.* **5,** e311
55. Christel, C. J., Schaer, R., Wang, S., Henzi, T., Kreiner, L., Grabs, D., Schwaller, B., and Lee, A. (2012) Calretinin regulates Ca^{2+}-dependent inactivation and facilitation of $Ca_v2.1$ Ca^{2+} channels through a direct interaction with the $\alpha_1 2.1$ subunit. *J. Biol. Chem.* **287,** 39766–39775
56. Berridge, M. J. (1990) Calcium oscillations. *J. Biol. Chem.* **265,** 9583–9586
57. Hajnóczky, G., Csordás, G., Das, S., Garcia-Perez, C., Saotome, M., Sinha Roy, S., and Yi, M. (2006) Mitochondrial calcium signalling and cell death: approaches for assessing the role of mitochondrial Ca^{2+} uptake in apoptosis. *Cell Calcium* **40,** 553–560
58. Chaudry, I. H. (1982) Does ATP cross the cell plasma membrane. *Yale J. Biol. Med.* **55,** 1–10
59. Dupont, G., Combettes, L., Bird, G. S., and Putney, J. W. (2011) Calcium oscillations. *Cold Spring Harb. Perspect. Biol.* **3,** a004226
60. Schwaller, B. (2014) Calretinin: from a "simple" Ca^{2+} buffer to a multifunctional protein implicated in many biological processes. *Front. Neuroanat.* **8,** 3
61. Schwaller, B., Celio, M. R., and Doglioni, C. (2004) Identification of calretinin and the alternatively spliced form calretinin-22k in primary pleural mesotheliomas and in their metastases. *Anticancer Res.* **24,** 4003–4009
62. Perocchi, F., Gohil, V. M., Girgis, H. S., Bao, X. R., McCombs, J. E., Palmer, A. E., and Mootha, V. K. (2010) MICU1 encodes a mitochondrial EF hand protein required for Ca^{2+} uptake. *Nature* **467,** 291–296
63. Waldeck-Weiermair, M., Jean-Quartier, C., Rost, R., Khan, M. J., Vishnu, N., Bondarenko, A. I., Imamura, H., Malli, R., and Graier, W. F. (2011) Leucine zipper EF hand-containing transmembrane protein 1 (Letm1) and uncoupling proteins 2 and 3 (UCP2/3) contribute to two distinct mitochondrial Ca^{2+} uptake pathways. *J. Biol. Chem.* **286,** 28444–28455
64. Marhl, M., Schuster, S., and Brumen, M. (1998) Mitochondria as an important factor in the maintenance of constant amplitudes of cytosolic calcium oscillations. *Biophys. Chem.* **71,** 125–132
65. Haynes, C. L., Buhler, L. A., and Wightman, R. M. (2006) Vesicular Ca^{2+}-induced secretion promoted by intracellular pH-gradient disruption. *Biophys. Chem.* **123,** 20–24
66. De Marchi, U., Santo-Domingo, J., Castelbou, C., Sekler, I., Wiederkehr, A., and Demaurex, N. (2014) NCLX protein, but not LETM1, mediates mitochondrial Ca^{2+} extrusion, thereby limiting Ca^{2+}-induced NAD(P)H

production and modulating matrix redox state. *J. Biol. Chem.* **289,** 20377–20385
67. Castaldo, P., Cataldi, M., Magi, S., Lariccia, V., Arcangeli, S., and Amoroso, S. (2009) Role of the mitochondrial sodium/calcium exchanger in neuronal physiology and in the pathogenesis of neurological diseases. *Prog. Neurobiol.* **87,** 58–79
68. Kaasik, A., Safiulina, D., Zharkovsky, A., and Veksler, V. (2007) Regulation of mitochondrial matrix volume. *Am. J. Physiol. Cell Physiol.* **292,** C157–C163
69. Schuster, S., Marhl, M., and Höfer, T. (2002) Modelling of simple and complex calcium oscillations. From single-cell responses to intercellular signalling. *Eur. J. Biochem.* **269,** 1333–1355
70. De Young, G. W., and Keizer, J. (1992) A single-pool inositol 1,4,5-trisphosphate-receptor-based model for agonist-stimulated oscillations in Ca^{2+} concentration. *Proc. Natl. Acad. Sci. U.S.A.* **89,** 9895–9899
71. Somogyi, R., and Stucki, J. W. (1991) Hormone-induced calcium oscillations in liver cells can be explained by a simple one pool model. *J. Biol. Chem.* **266,** 11068–11077
72. Dupont, G., and Goldbeter, A. (1993) One-pool model for Ca^{2+} oscillations involving Ca^{2+} and inositol 1,4,5-trisphosphate as co-agonists for Ca^{2+} release. *Cell Calcium* **14,** 311–322
73. Sneyd, J., Tsaneva-Atanasova, K., Yule, D. I., Thompson, J. L., and Shuttleworth, T. J. (2004) Control of calcium oscillations by membrane fluxes. *Proc. Natl. Acad. Sci. U.S.A.* **101,** 1392–1396
74. Bird, G. S., and Putney, J. W., Jr. (2005) Capacitative calcium entry supports calcium oscillations in human embryonic kidney cells. *J. Physiol.* **562,** 697–706
75. Lichtshtein, D., Kaback, H. R., and Blume, A. J. (1979) Use of a lipophilic cation for determination of membrane potential in neuroblastoma-glioma hybrid cell suspensions. *Proc. Natl. Acad. Sci. U.S.A.* **76,** 650–654
76. Houamed, K., Fu, J., Roe, M. W., and Philipson, L. H. (2004) in *Diabetes Mellitus: a Fundamental and Clinical Text* (LeRoith, D., Taylor, S. I., and Olefsky, J. M., eds) pp. 51–68, Lippincott, Williams, and Wilkins, Philadelphia
77. Walsh, C., Barrow, S., Voronina, S., Chvanov, M., Petersen, O. H., and Tepikin, A. (2009) Modulation of calcium signalling by mitochondria. *Biochim. Biophys. Acta* **1787,** 1374–1382
78. Pecze, L., Blum, W., and Schwaller, B. (2013) Mechanism of capsaicin receptor TRPV1-mediated toxicity in pain-sensing neurons focusing on the effects of Na^+/Ca^{2+} fluxes and the Ca^{2+}-binding protein calretinin. *Biochim. Biophys. Acta* **1833,** 1680–1691
79. Ducreux, S., Gregory, P., and Schwaller, B. (2012) Inverse regulation of the cytosolic Ca^{2+} buffer parvalbumin and mitochondrial volume in muscle cells via SIRT1/PGC-1α axis. *PLoS One* **7,** e44837
80. Schwaller, B. (2012) The regulation of a cell's Ca^{2+} signaling toolkit: the Ca^{2+} homeostasome. *Adv. Exp. Med. Biol.* **740,** 1–25
81. Doglioni, C., Dei Tos, A. P., Laurino, L., Iuzzolino, P., Chiarelli, C., Celio, M. R., and Viale, G. (1996) Calretinin: a novel immunocytochemical marker for mesothelioma. *Am. J. Surg. Pathol.* **20,** 1037–1046
82. Lukas, W., and Jones, K. A. (1994) Cortical neurons containing calretinin are selectively resistant to calcium overload and excitotoxicity *in vitro*. *Neuroscience* **61,** 307–316
83. Gotzos, V., Wintergerst, E. S., Musy, J. P., Spichtin, H. P., and Genton, C. Y. (1999) Selective distribution of calretinin in adenocarcinomas of the human colon and adjacent tissues. *Am. J. Surg. Pathol.* **23,** 701–711
84. Gander, J.-C., Bustos-Castillo, M., Stüber, D., Hunziker, W., Celio, M., and Schwaller, B. (1996) The calcium-binding protein calretinin-22k, an alternative splicing product of the calretinin gene is expressed in several colon adenocarcinoma cell lines. *Cell Calcium* **20,** 63–72
85. Boyer, J., Allen, W. L., McLean, E. G., Wilson, P. M., McCulla, A., Moore, S., Longley, D. B., Caldas, C., and Johnston, P. G. (2006) Pharmacogenomic identification of novel determinants of response to chemotherapy in colon cancer. *Cancer Res.* **66,** 2765–2777
86. Hrabakova, R., Kollareddy, M., Tyleckova, J., Halada, P., Hajduch, M., Gadher, S. J., and Kovarova, H. (2013) Cancer cell resistance to aurora kinase inhibitors: identification of novel targets for cancer therapy. *J. Proteome Res.* **12,** 455–469
87. Blum, W., and Schwaller, B. (2013) Calretinin is essential for mesothelioma cell growth/survival *in vitro*: a potential new target for malignant mesothelioma therapy? *Int. J. Cancer* **133,** 2077–2088
88. Gander, J. C., Gotzos, V., Fellay, B., and Schwaller, B. (1996) Inhibition of the proliferative cycle and apoptotic events in WiDr cells after down-regulation of the calcium-binding protein calretinin using antisense oligodeoxynucleotides. *Exp. Cell Res.* **225,** 399–410